ADDIS ABABA UNIVERSITY

ADDIS ABABA INSTITUTE OF TECHNOLOGY

SCHOOL OF CIVIL AND ENVIRONMENTAL ENGINEERING

A Study of Relationship between Seismic Provision and Progressive Collapse Resistance

Thesis Submitted to Postgraduate Studies in Partial Fulfillment

of the Requirements for the Degree of Master of Science

in Structural Engineering

By Mikiyas Dasa

December, 2018

Addis Ababa, Ethiopia

The undersigned have examined the thesis entitled 'A **Study of Relationship Between Seismic Provision and Progressive Collapse Resistance**' presented by **Mikiyas Dasa**, a candidate for the degree of **Master of Science** and hereby certify that it is worthy of acceptance.

Dr. -Ing. Adil Zekaria		
Advisor	Signature	Date
Internal Examiner	Signature	Date
External Examiner	Signature	Date
Chair person	Signature	Date

UNDERTAKING

I certify that research work titled "**A Study of Relationship between Seismic Provision and Progressive Collapse Resistance**" is my own work. The work has not been presented elsewhere for assessment. Where material has been used from other sources it has been properly acknowledged.

Mikiyas Dasa

ABSTRACT

Progressive collapse is known to be the cause of most catastrophic structural failures around the world. Recent acts of terrorism including the destruction of the World Trade Center demand for methods to improve behavior of structures under these abnormal events. Design of structures against progressive collapse has not been an integral part of structural design. However, some codes such the GSA and UFC guideline have detail requirements to reduce the likelihood of progressive collapse. Effect of seismic provision in progressive collapse resistance was not mentioned in this guidelines.

Hence, one of this thesis aim was to investigating the relationship between seismic provision and progressive collapse resistance of RC framed structures. To achieve this, a six-story regular RC framed models were designed according to ES EN 1998:1-2015. Ground accelerations of 0.15g with low, medium and high ductility classes were used. Moreover, a deficient structure with insufficient development length and lap splice at connection was also considered. Progressive collapse analysis was carried out on the four structures by considering four different column loss scenarios. Nonlinear static (pushdown) analysis were adopted in all 16 cases of progressive collapse assessment based on GSA 2013 guidelines.

It was concluded that the progressive collapse resistance of a structure is influenced heavily by the design ductility. Buildings designed for lower ductility have higher yield loads but undergo lower deformations before collapse. On the other hand, buildings designed for higher ductility yield at lower loads but they undergo greater deformations and absorbs more energy to resist collapse. However, based on the progressive collapse analysis low ductility design is the one that perform good in progressive collapse with maximum load factor when compared with medium and high ductility design.

The other aim of this thesis was to study the development of CAA and CA analytical model for beam column sub-assemblage, and to investigate application of CAA into alternative path design. It was found that the analytical model was quite similar with experimental result and it shows that reinforced concrete beams can be modeled as rigid rectangular blocks between the hinge locations to determine CAA and CA capacity. In addition, with adequate boundary restraints and shear strength, CAA found to be applicable into the design against progressive collapse.

ACKNOWLEDGMENTS

First of all, I would like to thank God for the time and the patience He gave me for completing this thesis.

Next, I would like to thank my advisor, **Dr.-Ing. Adil Zekaria** who had given me his full support in guiding me with motivating suggestions and encouragement to go ahead in all the time of the thesis work.

I also extend my gratitude towards my friends for their support and help. In particular, I am very much thankful of **Mr.Tizazu Geremew** who helped me in providing information and idea in the development of the thesis document.

Special thanks for Addis Ababa Institute of Technology and Ethiopian Road Authority for academic sponsor.

At last but not the least my gratitude towards my parents for continually supporting me throughout my studies and pushing me to do my best.

TABLE OF CONTENTS

UNDERTAKING ..... **III**

ABSTRACT ..... **IV**

ACKNOWLEDGMENTS ..... **V**

LIST OF TABLES ..... **IX**

LIST OF FIGURES ..... **IX**

CHAPTER 1 INTRODUCTION **1**

1.1 Overview 1

1.2 Statement of the Problem 1

1.3 Research Objectives 2

1.4 Scope of the Present Study 3

1.5 Organization of the Thesis 3

CHAPTER 2 LITERATURE REVIEW **4**

2.1 Progressive Collapse Definition 4

2.2 Cause of Progressive Collapse 4

2.3 Progressive collapse Example 5

2.4 Behavior of Structures under Collapse 6

2.5 Mechanisms to Prevent Progressive Collapse 7

2.5.1 Vierendeel action 7

2.5.2 Compression arch action (CAA) 8

2.5.3 Catenary action (CA) 8

2.6 Methods for Progressive Collapse Mitigation 9

2.7 US General Services Administration Guidelines 10

2.8 Progressive Collapse Analysis 11

2.9 Previous Research 13

2.9.1 Experimental studies 14

2.9.2 Numerical studies 15

CHAPTER 3 DESIGN OF RC MOMENT RESISTING FRAME **17**

3.1 Description of Structural Systems 17

3.2 Analytical Modelling with ETABS 19

3.3 Design Loads and Combinations 19
3.3.1 Load cases 19
3.3.2 Design load combinations 21
3.3.3 Seismic load parameters 21
3.3.4 Analysis verification and 2nd order effects 22
3.3.5 Design results 23
CHAPTER 4 PROGRESSIVE COLLAPSE ANALYSIS 25
4.1 Nonlinear Static (Pushdown) Analysis 25
4.1.1 Plastic hinge properties for seismically design buildings 26
4.1.2 Rotational limit 27
4.1.3 Plastic hinge properties for deficient detailing 27
4.2 Results and Discussion 28
4.2.1 Axial load redistribution 28
4.2.2 Pushdown result 33
4.2.3 Plastic hinges rotations 37
4.2.4 Effects of structural deficiencies (poor detailing) 38
CHAPTER 5 ANALATICAL STUDY 39
5.1 Introduction 39
5.2 Simplified Methods of Modeling Compressive Arch Action (CAA) 40
5.3 Simplified Methods of Modeling Catenary Action (CA) 49
5.4 Bar Fracture 52
5.5 Result and Discussion 53
5.5.1 Evaluation of the proposed model 53
5.5.2 Effect of seismic provision on the development of CAA and CA 56
5.5.3 Application of compressive arch action (CAA) into design 59
CHAPTER 6 CONCLUSIONS AND RECCOMENDATIONS 63
6.1 Summary 63
6.2 Conclusion 64
6.3 Recommendation for Future Work 65

REFERENCES **66**

APPENDIX A: SIMPLIFICATION OF THE COMPATIBILITY EQUATIONS. **68**

APPENDIX B: ESTIMATION OF RESTRAINT STIFFNESS **70**

APPENDIX C: EXPERIMENT RESULTS USED FOR COMPARISON **74**

APPENDIX D: AXIAL LOAD DISTRIBUTION BEFORE AND AFTER REMOVAL OF COLUMN **76**

APPENDIX E: VERIFICATION OF PUSHDOWN ANALYSIS USING ETABS **77**

LIST OF TABLES

Table 2.1: Nonlinear modeling parameters and acceptance criteria for reinforced concrete beams (GSA, 2013)..... 13
Table 3.1: Member cross-section dimensions..... 18
Table 3.2: Material partial factors of safety..... 19
Table 3.3: Values of horizontal response spectrum..... 21
Table 3.4**:** Behavior factors used for the analysis. 21
Table 3.5: Analysis output and drift sensitivity check in y direction..... 22
Table 3.6: Sample beam detailing for Axis 1 first floor..... 24
Table 3.7: Bottom story column reinforcement..... 24
Table 4.1: Percentage redistribution of axial loads in Case 1..... 32
Table 4.2: Percentage redistribution of axial loads in Case 2..... 32
Table 4.3: Percentage redistribution of axial loads in Case 3..... 32
Table 4.4: Percentage redistribution of axial loads in Case 4..... 32
Table 4.5: Maximum load factors..... 36
Table 4.6: Maximum plastic hinge rotations (radians)..... 37
Table 5.1: Comparison of experimental and theoretical results for CAA and CA models. 55
Table 5.2: Comparison of ductility class effect for CAA and CA capacity..... 58
Table 5.3: Structural deformation corresponding to CAA capacity (experiment result) 60
Table 5.4: Structural deformation corresponding to CAA capacity (analytical result)... 60
Table 5.5: Considering with and without CAA..... 62
Table C.1: Geometric properties of sub-assemblage specimens and experimental results of (Yu and Tan, 2013 & Yu and Tan, 2010)..... 74
Table C.2: Geometric properties of sub-assemblage specimens and experimental results (Alogla, 2016)..... 74
TableD.1: Axial load distribution before removal of column (kN)..... 76
Table D.2: Axial load redistribution for Case 1 (kN)..... 76
Table D.3: Axial load redistribution for Case 2 (kN)..... 76
Table D.4: Axial load redistribution for Case 3 (kN)..... 76
Table D.5: Axial load redistribution for Case 4 (kN)..... 76

LIST OF FIGURES

Figure 2.1: Ronan Point building after collapse (Pearson, 2005) 5
Figure 2.2: Murrah Federal Office Building after 19 April 1995 attack (Corley, 1998) .. 6
Figure 2.3: Change in bending moment diagram due to loss of column (Orton, 2007).... 7
Figure 2.4: Vierendeel action (Orton, 2007) 7
Figure 2.5: Compressive arch action (Rankin, 1997)..... 8
Figure 2.6: Catenary tension forces (Orton, 2007)..... 8
Figure 2.7: (a) Flow of force before damage (b) Flow of force after damage 10
Figure 2.8: Loads and load locations for external and internal column removal for linear and nonlinear static models 12
Figure 2.9: The collapse mode of the specimen (Yu and Tan, 2013) 14
Figure 2.10: The relationship of the applied force to the MJD (Yu and Tan, 2013)..... 15
Figure 2.11: Free body diagram of Orton's Model (Orton, 2007) 16
Figure 3.1: Building plan..... 17
Figure 3.2: Stress-strain model for steel-confined concrete (Mander et al, 1988)..... 20
Figure 3.3: Rebar stress-strain curve (Mander et al, 1988)..... 20
Figure 3.4: Beam detailing 23
Figure 4.1: Location of column removal..... 25
Figure 4.2: Plastic hinge property as per GSA guidelines 26
Figure 4.3: Typical frame with deficient reinforced beam and location of plastic hinge 28
Figure 4.4 Bending moments (kNm) (a) before and (b) after loss of column (Case 1) .. 29
Figure 4.5: Axial force (kNm) (a) before and (b) after loss of column (Case 1) 30
Figure 4.6: Deformed shape of frame after loss of column (Case 1) (a) Axis 1 (b) Axis C 31
Figure 4.7: Plastic hinge formation for high ductility design, Axis 1 (Case 1)..... 33
Figure 4.8: Pushdown curve for Case 1 34
Figure 4.9: Pushdown curve for Case 2 34
Figure 4.10: Pushdown curve for Case 3 35
Figure 4.11: Pushdown curve for Case 4 35
Figure 5.1 Arching action..... 39
Figure 5.2: Load-deflection relationship for RC slabs with edges restrained against lateral movement (Park, 1964) 40

Figure 5.3: Beam-column sub-assemblage with a concentrated load (Yu and Tan, 2014) 40
Figure 5.4 Free body diagrams of RC beam under CAA (a) One-bay beam (b) Middle joint (Yu and Tan, 2014) 41
Figure 5.5 Equivalent boundary conditions for a two-bay beam (Yu and Tan, 2014).... 42
Figure 5.6: Compatibility conditions of beam-column sub-assemblage (Yu and Tan, 2014)..... 43
Figure 5.7: Strain and stress distribution at a beam section (Yu and Tan, 2014)..... 46
Figure 5.8: Beam deflation shape at catenary stage 49
Figure 5.9: Deflection compatibility 50
Figure 5.10: Idealized steel stress-strain model 51
Figure 5.11: Deflected shape of single bay beam after bar fracture..... 53
Figure 5.12: Comparison of analytical and experimental value for (Yu and Tan, 2013) S4..... 54
Figure 5.13: Comparison of analytical and experimental value for (Yu and Tan, 2013) S6..... 54
Figure 5.14: Location of analyzed beam 56
Figure 5.15: Load deflection relationship for Case 1 57
Figure 5.16: Load deflection relationship for Case 2 57
Figure 5.17: Load deflection relationship of Case 4 58
Figure 5.18 Moment-rotation relationship of a plastic hinge with CAA 61
Figure 5.19: Pushdown of medium ductility design for Axis 1 62
Figure B.1: Adjacent members in the spreading of bending moment (Hải, 2009) 70
Figure B.2: Three levels development of at point C (Hải, 2009)..... 71
Figure B.3: Horizontal restraint definition (Hải, 2009)..... 72
Figure B.4: The development of the model and its stiffness (Hải, 2009) 73
Figure C.1: Detailing and boundary conditions of specimens (Unit: mm) (Yu and Tan 2013)..... 75
Figure C.2: Geometric properties of sub-assemblage specimens (Alogla, 2016) 75
Figure E.1: (a) Plan frame used for verification (b) Base shear vs middle joint displacement..... 77

LIST OF SYMBOLS

$a_{s1,}a_s$ Concrete cover at the tension side of beam end and middle joint

$a_{s1}^{'}, a_s^{'}$ Concrete cover at the Compression side of beam end and middle joint

$A_s, A_s^{'}$ Area of tensile and compression reinforcement

A_{st}, A_{sb} Top and bottom reinforcement area

$A_{s,Ava}$ Average reinforcement area of top and bottom

b Width of a beam section

b_j Width of a middle joint

CAA, CA Compression arch action and Catenary action

c, c_1 Neutral axis depth at the middle joint interface and at the beam end

$C_c^{'}, C_c$ Concrete compressive force acting at the beam end and the middle joint interface

$C_s^{'}, C_s$ Steel compressive force acting at the beam end and the middle joint interface

d Effective depth of a beam section

d_b Diameter of a reinforcing bar

E_c Elastic modulus of concrete

E_s Elastic modulus of steel reinforcement

f_s Applied stress at the loaded end of a bar

f_y, f_u Yield strength and ultimate tensile strength of reinforcement

$f_c^{'}$ Compressive strength of concrete

G Gravity loads for floor areas away from removed column

G_N Increased gravity loads for deformation-controlled actions for Linear Static analysis

G_{ND} Gravity loads for nonlinear dynamic analysis

h Depth of a beam section

K_a, K_r Stiffness of axial and rotational restraints

l Total net span length of sub-assemblages

l_n Net span length of a one-bay beam

l_1 Crack width at an end of a sub-assemblage

L_n Net span length of a single-bay beam

L Total net span length of a sub-assemblage

L_p Plastic hinge length

M_{u1}, M_u Bending moments acting on the beam end and on the joint interface

M Bending moment at a beam section

MJD Middle joint displacement

N Axial force at a beam section

N_u, N_{ul} Axial force acting on the beam end and on the joint interface

N_{top}, N_{bottom} Top and bottom axial force

P Progressive collapse (or vertical) resistance of sub-assemblages

p_f Calculated flexural capacity based on plastic hinge mechanism

P_{caa} Experimental compressive arch action capacity

t Outward and inward lateral displacement of beam end

t_o Gap between axial restraints and beam ends

T', T Steel tensile force acting at beam end and joint interface

V Shear force at a middle joint interface

β Ratio of the net span length of a single-bay beam to the total net span length

β_1 Ratio of the depth of the equivalent rectangular stress block to the neutral-axis depth

δ Beam deflection or displacement at the middle joint

δ_g Axial extension

ε_{cu} Ultimate compressive strain of concrete, assumed as 0.003

ε_s' Strain of compression reinforcement

ε_y Yield strain of steel reinforcement

ε_E Strain due to elongation

ε_R Strain due to rotation

μ Enhancement factor of structural capacity due to compressive arch action

θ Rotation at a beam section

θ_y, θ_u Yield and ultimate rotation of plastic hinges

θ_{pra} Plastic rotation angle

φ Rotation at the end support

Ω_N Dynamic increase factor

CHAPTER 1 INTRODUCTION

1.1 Overview

Progressive collapse, as will be defined more accurately in the next chapter, is the term used to describe the spread of initial local failure like a chain reaction, leading to the partial or total collapse of a structure. The basic characteristic of progressive collapse is that the failure at the final stage is disproportionately greater than the failure that initiated the collapse. Collapse can be triggered by many different actions. These include earthquakes, explosions caused by gas or explosives, impacts of vehicles and planes and human errors in design or construction. It begins with the failure of one or more structural members, which triggers a load transfer to the adjacent members. If the capacity of these members is not enough to resist these additional loads, they also fail triggering further redistribution of load. This chain reaction continues until the collapsing portion is completely separated from the remaining structure (GSA, 2003).

To save lives and improve structural safety, progressive collapse analysis has become important to civil engineers. Design guidelines for progressive collapse analysis like The General Services Administration (GSA) published design guidelines (in 2003 and amended in 2013) for Progressive collapse resistance and provided detailed analysis recommendations, which are discussed in the literature review. In 2005 & 2009, the United States Department of Defense (DoD) has also published Unified Facilities Criteria (UFC) addressing progressive collapse resistance and analysis. These guidelines recommend the alternate path method for analyzing a structure for its progressive collapse vulnerability. The alternate path analysis method involves removing a column from four specified locations and conducting a collapse analysis. The limit states of the elements are then checked and collapse potential is assessed per a given criteria.

1.2 Statement of the Problem

In seismic design, building can be designed with different energy dissipation level that means, with different combination of strength and ductility. And effect of designing with these different combination in progressive collapse resistance is not well known and required a study.

Vulnerability of deficient existing structure in progressive collapse are not fully addressed. Deficient structure can be defined as an old concrete structure constructed before the more stringent provisions for seismic resistance and structural integrity in current code requirements, and also build having low reinforcement detailing quality. Deficient structure have short embedment length of bottom beam reinforcement (positive moment) at column supports. These deficiencies may prevent the development of alternate load paths when elements are damaged or destroyed and may lead to progressive collapse.

1.3 Research Objectives

The overall goal of this research is to understand the vertical load carrying capacity of reinforced concrete structures in progressive collapse. And investigate the progressive collapse potential of RC frame structures designed to ES EN 1998:1-2015 with different seismic energy dissipation levels. Since compressive arch action and catenary action are the main progressive collapse resistance mechanism after flexural action. It is required to study effect of seismic design in the development of this member forces.

Specific objectives are:

- Investigate the influence of designing with different energy dissipation capacity (ductility classes), and column removal locations on the progressive collapse potential of seismically designed RC frame structures, using the nonlinear static (pushdown) analysis procedures according to GSA (2013) guideline.
- To compare alternative load path capacity of Robust and Deficient structures.
- To investigate the development of CAA and CA in reinforced concrete beam using theoretical numerical model and effect of seismic design in the development of those member forces.
- To develop and modify CAA and CA analytical model by including bar fracture as additional factor.
- To investigate application of CAA into alternative path design, since with adequate lateral restrain CAA of RC beams can mobilize prior to CA. The presence of axial compression in beams at CAA stage could enhance structural resistance at relatively small deflection. If the deflection corresponding to CAA capacity is less than allowed

deflection limit in the design guidance, then CAA can confidently incorporate into the alternative load path design method.

1.4 Scope of the Present Study

- The research focused on the moment resisting reinforced concrete frame building
- For progressive collapse analysis only nonlinear static analysis is conducted, dynamic effect was introduced through dynamic increase factors (DIF) only.
- Based on Studies of Yu and Tan (2013), the progressive collapse of RC framed structures is controlled by the flexural failure of beams. Therefore, only flexural failure hinges were used for beams.

1.5 Organization of the Thesis

Chapter 1 presents a general introduction to the concept of progressive collapse, the motivation and objectives of this research.

Chapter 2 gives a detailed review on the principles of progressive collapse and a review of the guidelines given by the GSA (2013) for progressive collapse mitigation. Previous research works relating to progressive collapse analysis are also presented here.

Chapter 3 presents a description of the configuration of the study buildings. Member sizes and material properties used in the design are described. It also defines the seismic loading parameters used for the design to ES EN 1998:1-2015.

Chapter 4 presents the progressive collapse modelling parameters and procedures used in the nonlinear static (pushdown) analysis. And the responses of the structures to the loss of the columns are discussed in detail.

Chapter 5 presents analytical study of beam adjacent to fail column under column removal scenario. The analytical study includes the development of Compressive arch action (CAA) and catenary action (CA) models and also presents implementation of CAA in the alternative path design.

Chapter 6 presents a summary of the work and major findings. Recommendations for future work are also described here.

CHAPTER 2 LITERATURE REVIEW

Many research works have been conducted on the subject of progressive collapse leading to a number of codes and standards for progressive collapse assessment. This chapter presents a literature review on the phenomenon of progressive collapse of building structures. The current state-of-art on progressive collapse is investigated by reviewing design guidelines and research works conducted on the subject.

2.1 Progressive Collapse Definition

The term progressive collapse describes a chain reaction of structural failures that occurs following damage caused by a relatively small portion of a structure; the damage that ultimately results is disproportionately large when compared with the mechanism that starts the chain reaction. The disproportionality refers to the situation in which failure of one member causes a major collapse, with a magnitude disproportionate to the initial event. The General Services Administration (GSA) defines progressive collapse phenomenon as "an extent of damage or collapse that is disproportionate to the magnitude of the initiating event."

2.2 Cause of Progressive Collapse

A number of potential abnormal load hazards, which could trigger progressive collapse, are considered in the following paragraphs. These hazards have a low probability of occurrence and are either not considered in structural design for economic reasons or addressed indirectly through passive protective measures rather than by structural calculations. Among the reasons are: general lack of meaningful load data, difficulty in identifying possible hazard scenarios; lack of any assurance that designing for specific loads would be effective in reducing the incidence of progressive collapse.

Abnormal loads may be grouped as pressure loads (e.g., explosions, detonations, tornado wind pressures), impact (e.g., vehicular collision, aircraft or missile impact, debris, swinging objects during construction or demolition), deformation-related (softening of steel in fire, foundation subsidence), or as faulty practice (NIST, 2007).

2.3 Progressive collapse Example

The collapse of the Ronan Point Tower in 1968 in Canning Town, London is one of the most famous cases of disproportionate collapse. The incident was initiated by a gas-stove leak on the 18th floor in apartment 90. The ultimate result was a collapse of the corner bay of the building from top to bottom. Ronan Point was a 22-story residential apartment tower consisted of precast panels joined together without a structural frame. Due to poor connections between the walls and floor, no alternate load paths to redistribute forces existed in the event of a partial collapse. Since the collapse of the southeast corner of Ronan Point, changes to building codes to prevent the recurrence of such tragedies have been initiated in the United Kingdom and throughout the world (Pearson, 2005).

Figure 2.1: Ronan Point building after collapse **(Pearson, 2005)**

Another example of disproportionate collapse is the Alfred P. Murrah Building in Oklahoma City, Oklahoma. The Murrah building was destroyed by a bomb on April 19, 1995. The bomb, in a truck at the base of the building, destroyed or badly damaged three columns. Loss of support from these columns led to failure of a transfer girder. Failure of the transfer girder caused the collapse of columns supported by the girder and floor areas supported by those columns. The result was a general collapse; about half of every floor was lost over the full height of the building. The building was designed with non-continuous reinforcement in both the positive and negative moment reinforcement in the beams (Corley, 1998).

Figure 2.2: Murrah Federal Office Building after 19 April 1995 attack **(Corley, 1998)**

2.4 Behavior of Structures under Collapse

During collapse, the structure could go through different seniors. For example, in the case studied by Orton 2007, the building experienced the loss of an exterior non-corner column, which not only caused significantly increased (approximately 4 times) bending moment due to the double span but also caused to reverse the moment direction over the missing column. Therefore, the regions that had been designed for negative moment encountered a positive moment and vice versa.

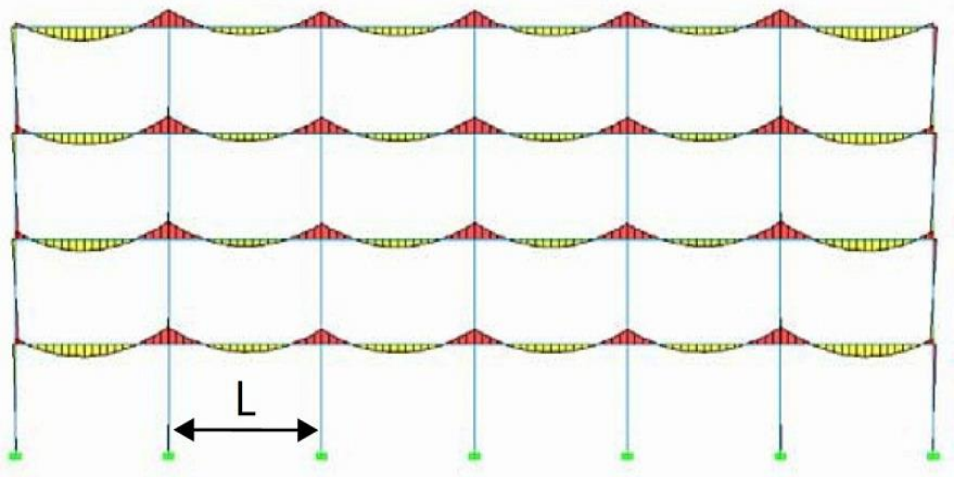

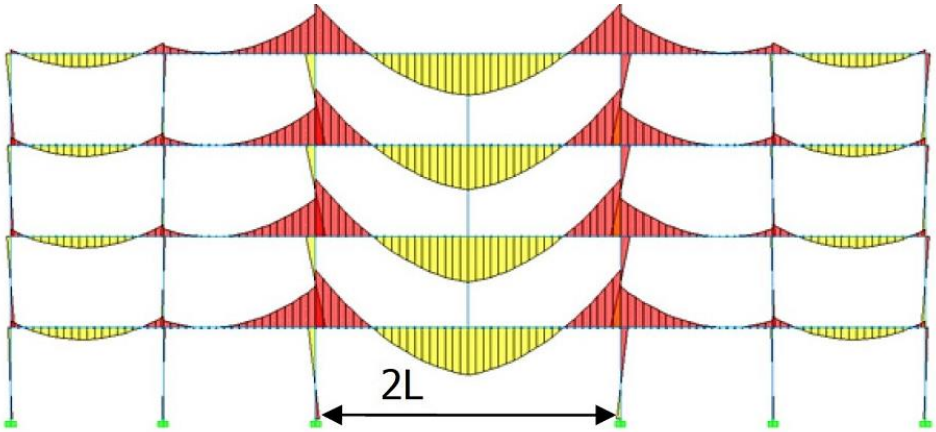

Figure 2.3: Change in bending moment diagram due to loss of column **(Orton, 2007)**

2.5 Mechanisms to Prevent Progressive Collapse

Mechanisms to prevent progressive collapse includes: Flexural Action (bending in beams), Vierendeel (frame) Action, Compressive Arch Action (CAA), and Catenary Action (CA).

2.5.1 Vierendeel action

This action, which is sometimes called Frame Action, basically develops due to the moment resistance that is generated in the beam-column connection of the building during the collapse. Vierendeel action can also be characterized by the relative vertical displacement between the beams ends and the corresponding double curvature deformations of the beams.

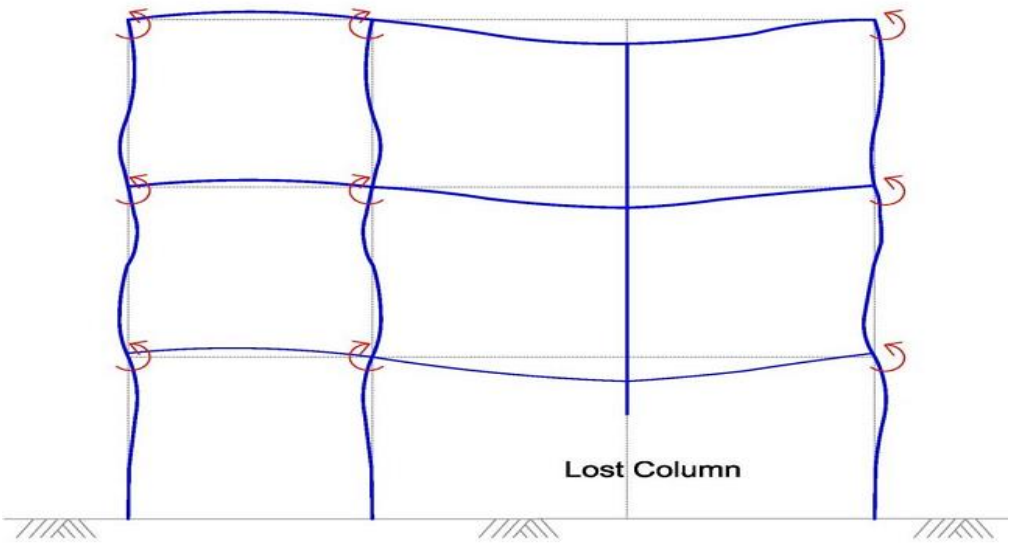

Figure 2.4: Vierendeel action **(Orton, 2007)**

2.5.2 Compression arch action (CAA)

Due to the axial restraint from the elements that are not affected by the collapse, beams or slabs that have been supported by the damaged column go at early stages of the collapse through a compressive arch action until the effect of the constraints vanishes. The effect of constraints starts to vanish when the beam starts to go through higher range of deflection. At large deflection, the axial force in the beam starts to be tensile, which indicates the beginning of the next stage: catenary action.

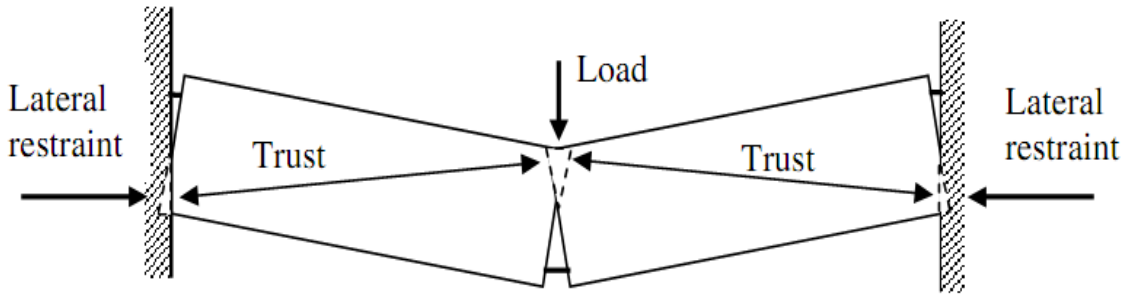

Figure 2.5: Compressive arch action **(Rankin, 1997)**

2.5.3 Catenary action (CA)

At large deformation and depending on the reinforcement details of the beam, catenary action may develop after compressive arch action. Catenary action depends mainly on the tensile force of longitudinal reinforcement to withstand the vertical loading. Catenary action, however, only becomes effective at large levels of displacement because the amount of vertical force is directly related to the angle of the beam.

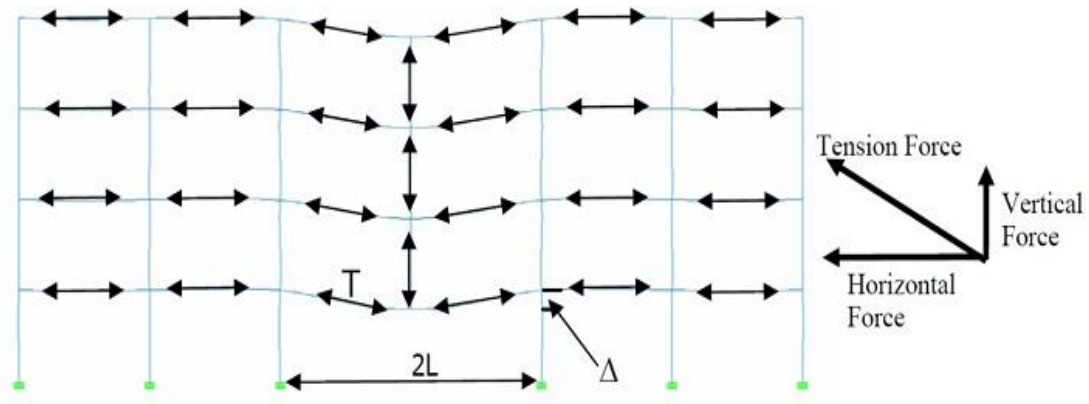

Figure 2.6: Catenary tension forces (Orton, 2007)

According to previous research, catenary action begins at large deformation. Orton (2007) found that the catenary effect does not occur until after the beam has reached its maximum extension, or until the deflection is equal to the height of the beam.

2.6 Methods for Progressive Collapse Mitigation

Several approaches have been developed and implemented in the design standards to make the new and existing facilities more resistant to the risk of the progressive collapse due to the abnormal loads. These sorts of loads are extremely difficult to be defined. Therefore, the analysis procedures to evaluate the progressive collapse are established in such a way that it may not always consider loading from those triggered events. The different design approaches used in progressive collapse are listed below.

a. Event control

The event control design method is used to mitigate or prevent the risk of progressive collapse by considering indirect actions to protect the buildings by eliminating the exposure to abnormal loads. For examples, isolation of parking zones, elimination of gas installation in multi-story structures.

b. Indirect control

Indirect approaches to progressive collapse neither define a threat nor assume a damaged state. These approaches require limited calculations and some resistance to progressive collapse can be indirectly attained through provision of minimum levels of strength, continuity, and ductility. Use of redundant structural systems that are capable of developing alternate load paths, if local damage occurs.

c. Direct control

The abnormal loads are considered in this design approach to resist the progressive collapse in structures. This is done by adopting specific provisions for the design of major elements such as load-carrying members, connections, and beams to provide a good structural performance in the progressive collapse situation. The alternate load path method and the specific local resistance method are the two design approaches that fall under the direct design procedure (NIST, 2007).

Alternate load path method

This design approach is primarily endorsed in the current analysis and design standards associated with progressive collapse phenomenon. Since this method is mainly recommended by the Department of Defense (DoD, 2010) and General Services Administration (GSA, 2013) which are the most two eminent guidelines in this realm, this research has been carried out by implementing the alternate load path method.

The philosophy of this method is to permit the occurrence of the local damage; however, the collapse of large portion of the structure is avoided by providing alternate load paths in the neighboring elements to redistribute the loads that were applied on the damaged components, if they have designed sufficiently (Figure 2.7). Finally, prevent any major failure happening in the facility.

From analytical point of view, exploitation of this method is done by applying the design loads and then different scenarios of instantly removing for one load-carrying member are performed. Last step of this design approach is done by evaluating the capacity of the remaining structure to resist the subsequent failure.

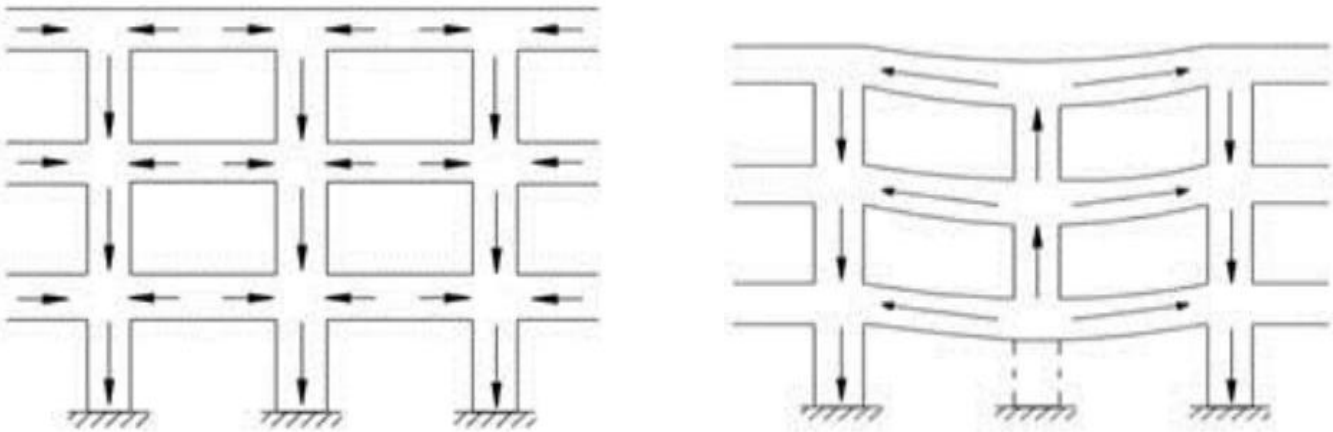

Figure 2.7: (a) Flow of force before damage (b) Flow of force after damage

2.7 US General Services Administration Guidelines

General Service Administration (GSA) in 2013 published a guidelines entitled “General Service Administration Alternative Path Analysis & Design Guidelines for Progressive Collapse.” The methodology proposed in GSA mainly focuses on the subsequent effects of

the abnormal loading on the structure, which is known as threat-independent. Moreover, the requirements specified in GSA were developed to meet the provisions of the Security Criteria on the progressive collapse developed by the Interagency Security Committee (ISC). According to 2013 GSA, the application of the progressive collapse design depends on the required level of protection, which should be determined based on the number of stories and the Facility Security Levels (FSL) in accordance with ISC. There are five FSL levels specified in ISC, to ensure that security becomes an integral part of the planning, design and construction of new federal office buildings. It should be noted that progressive collapse design is not required for FSL I & II given the low occupancy and risk level associated with these types of facilities. However, the design is mandatory for FSL III & IV, and V; the details are as follows,

- FSL III & IV: for the buildings with four or more stories measured from the lowest point of exterior grade to the highest point of elevation. These facilities should implement both the Alternative Path and Redundancy Design Procedures.
- FSL V: GSA (2013) is applicable for all buildings regardless of the number of stories while the Redundancy Design Procedures do not need to be applied to these facilities.

2.8 Progressive Collapse Analysis

According to the 2013 GSA Guidelines, four types of analyses can be used in the assessment of the potential for progressive collapse of buildings, i.e., linear static analysis, linear dynamic analysis, nonlinear static analysis, and nonlinear dynamic analysis. For the purpose of the nonlinear analysis, including both dynamic and static, all the actions of the elements should be classified as either deformation or force-controlled actions according to the Guidelines.

Analysis considerations and loading criteria

For both linear and non-linear static analysis the following vertical load shall be applied downward.

- Apply the following increased gravity load combination to those bays immediately adjacent to the removed element and at all floors above the removed element

$$G_N = \Omega_N \left[1.2D + (0.5Lor0.2S)\right] \quad \text{..... (2.1)}$$

- Apply the following gravity load combination to those bays not loaded with G_{LD} as shown in figure. $G = 1.2D + (0.5Lor0.2S)$ ..... (2.2)

Where: G is gravity load, G_N is Increased gravity loads for deformation-controlled actions for Static analysis, D is dead load $\left(kN/m^2\right)$, L is live load, S is snow load Ω_N is Dynamic increase factor for nonlinear static analysis. For Reinforced Concrete frame building dynamic increase factor is given by $(\Omega_N) = 1.04 + 0.45/\left(\theta_{pra}/\theta_y + 0.48\right)$. Where θ_{pra} is the plastic rotation angle of connection (beam or slab) and θ_y is the yield rotation. To determine Ω_N for the analysis of the entire structure, choose the smallest ratio of θ_{pra}/θ_y for any primary element, component, or connection in the model within or touching the area that is loaded with the increased gravity load.

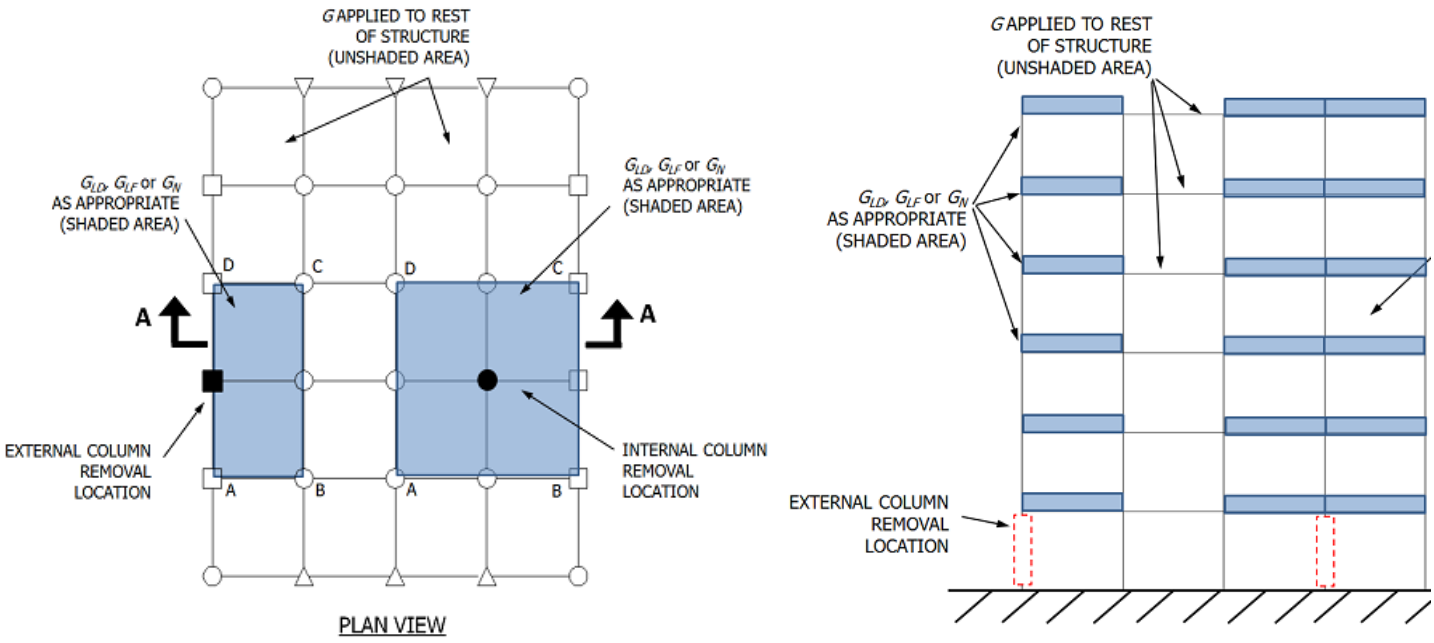

Figure 2.8: Loads and load locations for external and internal column removal for linear and nonlinear static models

Acceptance Criteria

The maximum allowable plastic rotations and ductility for a nonlinear analysis of reinforced concrete structure according to GSA (2013) given in the Table 2.1.

Table 2.1: Nonlinear modeling parameters and acceptance criteria for reinforced concrete beams (GSA, 2013)

Conditions			Modeling Parameters			Acceptance Criteria	
			Plastic Rotations Angle, radians		Residual Strength Ratio	Plastic Rotations Angle, radians	
			a	b	c	Primary Components	Secondary Components
i. Beams controlled by Flexural							
$\frac{\rho-\rho'}{\rho_{bal}}$	Trans.Reinf.[4]	$\frac{V}{b_w d\sqrt{f_c'}}$					
≤0.0	C	≤ 3	0.063	0.1	0.2	0.063	0.1
≤0.0	C	≥ 6	0.05	0.08	0.2	0.05	0.08
≥0.5	C	≤ 3	0.05	0.06	0.2	0.05	0.06
≥0.5	C	≥ 6	0.038	0.04	0.2	0.038	0.04
≤0.0	NC	≤ 3	0.05	0.06	0.2	0.05	0.06
≤0.0	NC	≥ 6	0.025	0.03	0.2	0.025	0.03
≥0.5	NC	≤ 3	0.025	0.03	0.2	0.025	0.03
≥0.5	NC	≥ 6	0.013	0.02	0.2	0.013	0.02
ii. Beams Controlled by shear							
Stirrups spacing ≤ d/2			0.003	0.02	0.2	0.003	0.02
Stirrups spacing ≥ d/2			0.003	0.01	0.2	0.003	0.01
iii. Beams controlled by inadequate development or splicing along the span							
Stirrups spacing ≤ d/2			0.003	0.02	0	0.003	0.02
Stirrups spacing ≥ d/2			0.003	0.01	0	0.003	0.01
iv. Beams controlled by inadequate embedment into beam-column joint							
			0.0015	0.03	0.2	0.0015	0.03

1. Linear interpolation between values listed in the Table shall be permitted
2. The definition of nonlinear modeling parameters a, b, and c. shown in Figure 4.2

2.9 Previous Research

Progressive collapse has been known for its catastrophic damages in buildings and people, it has been a topic of many research. Experimental and theoretical studies have been performed trying to fully understand this phenomenon and to enhance building resistance to progressive collapse. Due to the expense of experimental work, a few limited experimental tests are available, and some are discussed below.

2.9.1 Experimental studies

Yu and Tan (2013) study on six reinforced concrete axially strained beam column sub-assemblages, consisting of two single-bay beams, one middle joint and two end column stubs, were quasi-statically tested under a middle column removal scenario. The tests were aimed to investigate, if there are alternate load paths that can mitigate progressive collapse in related to reinforcement ratio through joints, reinforcement detailing at joint regions, and beam span-to-depth ratio on structural behavior of RC sub-assemblages.

Figure 2.9: The collapse mode of the specimen (Yu and Tan, 2013)

The test results gives, at structural levels, the relationships of applied loads vs. middle joint displacement (MJD) are used to represent the overall behavior, as shown in Figure 2.10. Based on the relationship of the applied force and the middle joint displacement of the specimen the classification of three different mechanisms, viz. flexural action, compressive arch action and catenary action, is shown in Figure below Flexural action develops until all plastic hinges occur at the critical sections. Catenary action kicks in at the moment of the applied force reversing and increasing again.

Jun Yu and Kang Hai Tan from the experiment concluded that with adequate axial and rotational restrains, the RC sub-assemblage develop compression arch action (CAA) and catenary action on top of flexural action. CAA capacity is 13.5%~43.2% larger than flexural action capacity calculated via conventional plastic hinge mechanism. The capacity of catenary action is 28%~128% greater than CAA capacity.

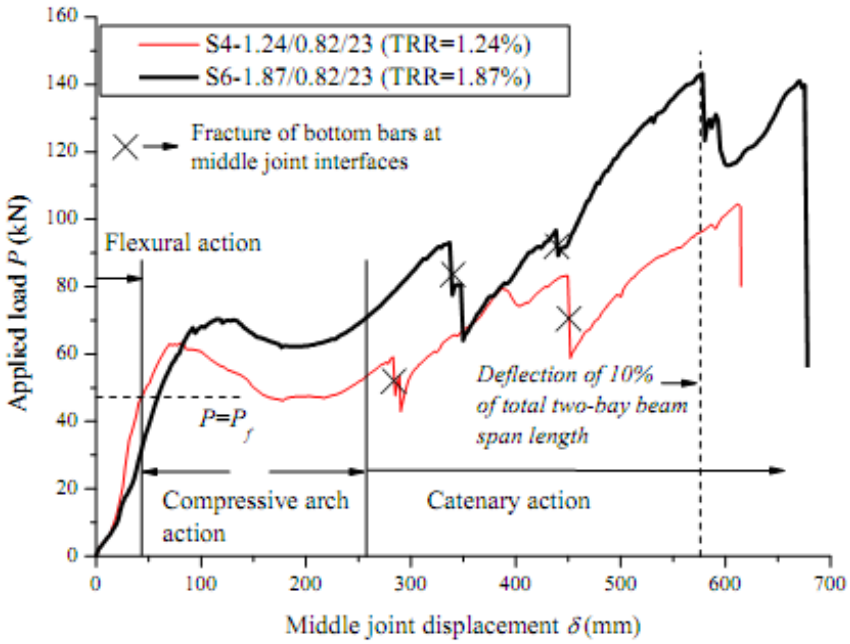

Figure 2.10: The relationship of the applied force to the MJD (Yu and Tan, 2013)

Orton (2007) studied eight beams in progressive collpase by using CFRP (carbon fibre reinforced polymer) sheets to increase the tension resistance as a possible method of retrofitting to enhance structural robustness. Orton concluded from the study that catenary action begins after the beam has formed a flexural failure mechanism, or the beam is no longer able to sustain additional vertical loads in a flexural manner" and "The deflection at which catenary action begins is directly dependent on the height of the beam."

2.9.2 Numerical studies

The numerical studies includes analytical study on continuous beams and progressive collapse analysis in three dimensional building.

Adrian M. Ioani (2013) studied the behavior of progressive collapse of a six-story RC framed building design for low, moderate and high (ag = 0.24 g) seismic area according to the provisions of the Romanian seismic code. A nonlinear static analysis was conducted in order to establish the progressive collapse resistance of the structural models. It was concluded that the RC frames seismically design on the progressive collapse resistance was quantified: the ultimate load bearing capacity of the structure designed for high seismic area is 7.3% higher than of the structure designed for a moderate seismic area, and is 38% higher than of the structure designed for low seismic area.

Yu and Tan (2014) numerically model a two span beam to predict compressive arch action capacity (CAA) capacity of RC beams by incorporate the actual stress state of compression reinforcement, rotational and axial restraints. The detail development of the proposed model by Yu and Tan explained in detail in the Chapter 4.

Orton (2007) developed a similar set of equations that were based on equilibrium, geometry (compatibility), and the axial extension of concrete beams. For a beam without continuous reinforcement, a hinge will open at the column line which has no moment capacity. Therefore, the equilibrium of the beam, with two point loads (see diagram in Figure 2.11), will be:

$$\sum M = 0 \qquad M + H\Delta - P\frac{L}{2} - P\frac{L}{2} = 0 \qquad H = \frac{PL - M}{\Delta} \quad \text{.....(2.4)}$$

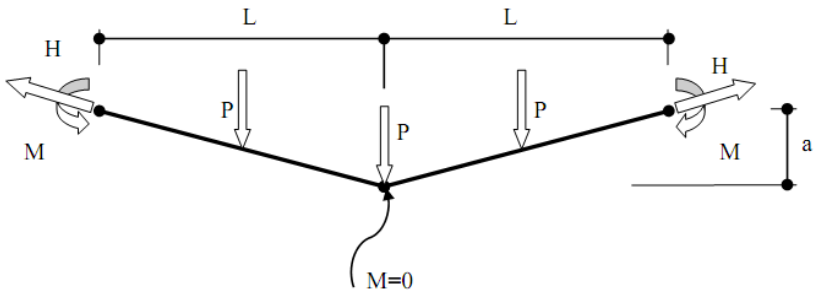

Figure 2.11: Free body diagram of Orton's Model (Orton, 2007)

Where M is the nominal flexural capacity, H is the axial tension, Δ is the center deflection, P is the point load, and L is the length of the modelled beam.

For the compatibility geometry, the extended length of the beam $(L + \Delta L)$ is related to the deflection Δ and original length L by the Pythagorean Theorem. Therefore, the equation becomes:

$$\Delta = \sqrt{\left((L + \Delta L)^2 - L^2\right)} \quad \text{..... (2.5)}$$

For axial extension, Orton considered three components: due to rotation of beam δ_g, support movement δ_s, and elongation in the beam δ_e. The equation has the following form:

$$\Delta L = \delta_g + \delta_s + \delta_e \quad \text{..... (2.6)}$$

CHAPTER 3 DESIGN OF RC MOMENT RESISTING FRAME

In this Chapter, the structural modelling, analysis and design of the buildings are presented. The structural system, member dimensions and material properties are described. The chapter also deals with the structural loading and the seismic data used in the analysis; structural regularity, design ductility classes and the related behavior factors. In all analysis cases, a spatial (3-D) model is used. All analyses were performed with the commercial finite element structural analysis software, ETABS.

3.1 Description of Structural Systems

Structural configuration and dimensions

In order to achieve the objectives, six-story reinforced concrete spatial frame models were considered. The robust structure were designed to ES EN 1998:1-2015 low, medium and high ductility provision with capacity design principle and the deficiency structure was designed to gravity load only plus with inadequate seismic provision.

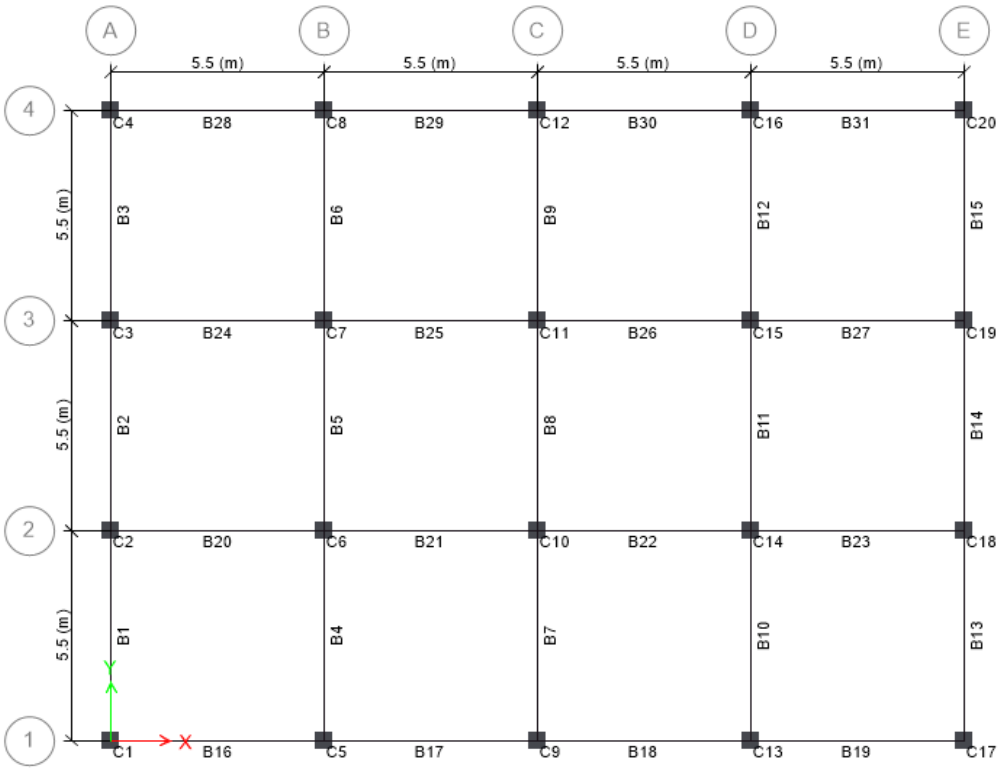

Figure 3.1**:** Building plan

Each building had four bays in the x-direction and three bays in the y-direction as shown in Figure 3.1. The structures were regular in plan and elevation. They had uniform column spacing of 5.5m giving an overall dimension of 22.0m in the x-direction and 5.5m in the y-direction giving an overall dimension of 16.5m. Story height is 3.2m for all floors giving a total building height of 19.2m. All beam-column connections were modelled as fully rigid whilst the foundations were modelled as fixed. Table 1 shows the detailed description of the member section dimensions used in the models. All dimensions are in millimeters.

Table 3.1: Member cross-section dimensions

Dimension	Columns (mm)	Beams (mm)	Slab (mm)
Height	450	450	150
Width	450	300	

Material properties

For all buildings, concrete strength of 30N/mm2 was used in all members. This is greater than the strength class C20/25 set as the minimum in the ES EN 1998:1-2015. The concrete had a modulus of elasticity of 31kN/mm^2 and a Poisson's ratio of 0.2. The unit weight of the concrete is 25kN/m^3.

For reinforced bar grade S400 was used with a yield strength of 400N/mm^2 and ultimate tensile stress of 600N/mm^2 for longitudinal reinforcement and grade S300 for the transverse reinforcement. Modulus of elasticity of reinforcement was 200kN/mm^2. Values for partial factors of safety as per ES EN used in the design are as shown in Table 2.

Table 3.2**:** Material partial factors of safety

Design Code	Member	Concrete (γc)	Reinforcing Steel (γs)
ES EN	Beam	1.5	1.15
	Column	1.5	1.15

3.2 Analytical Modelling with ETABS

The structure described was modelled with ETABS 2016.2.1, which is a stand-alone finite-element-based structural program for the analysis, and design of civil engineering structures. Rigid connection were used at the beam-column joints of the structural model. The effects of cracking were included by using reduced member stiffness, i.e., 50% of the gross E_cI for both beams and columns, where E_c is the modulus of elasticity of concrete and I is the moment of inertia of the member section. The moment-curvature relationship is evaluated using the steel and concrete stress strain curves. For seismically designed building a confined Mander et al (1988) concrete model, was used to model uniaxial constant confinement concrete stress-strain relationship, which shown in Figure 3.2. And for non-seismically designed building unconfined concrete model were used. Simple uniaxial stress-strain behavior of steel was used to model the reinforcement as shown in Figure 3.3.

3.3 Design Loads and Combinations

3.3.1 Load cases

The following static load cases were defined for the seismically designed buildings.

- Dead load (G_k): calculated automatically by the program based on the volume of the element and unit weight of the material.
- Live load (Q_k): 3.0kN/m^2 corresponding to a typical office for general use and is applied to all floors.

- Superimposed dead load which is considered in the design was 2.52kN/m^2, which included the loads due to floor finishing, partitions, and suspended ceiling. And peripheral wall load with 6.72kN/m^2 was used.
- Earthquake load is calculated by the ETABS program using the seismic data given.

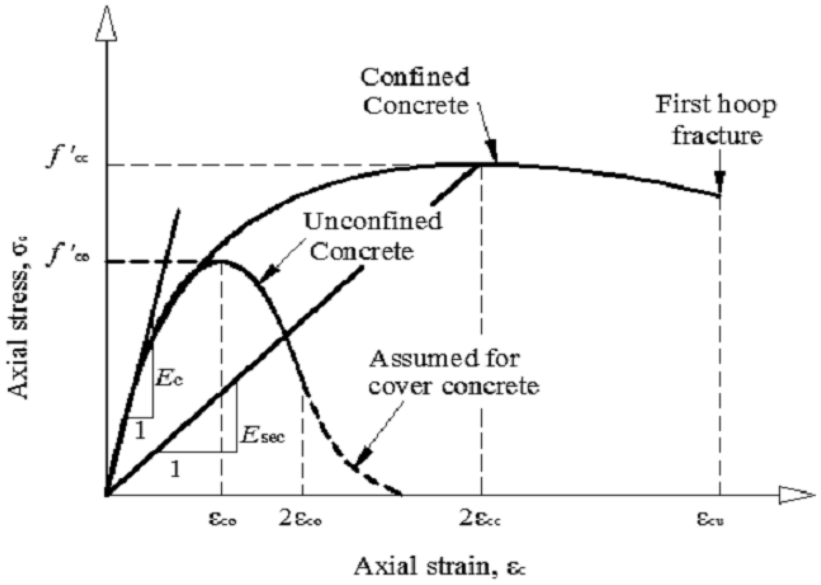

Figure 3.2: Stress-strain model for steel-confined concrete (Mander et al, 1988)

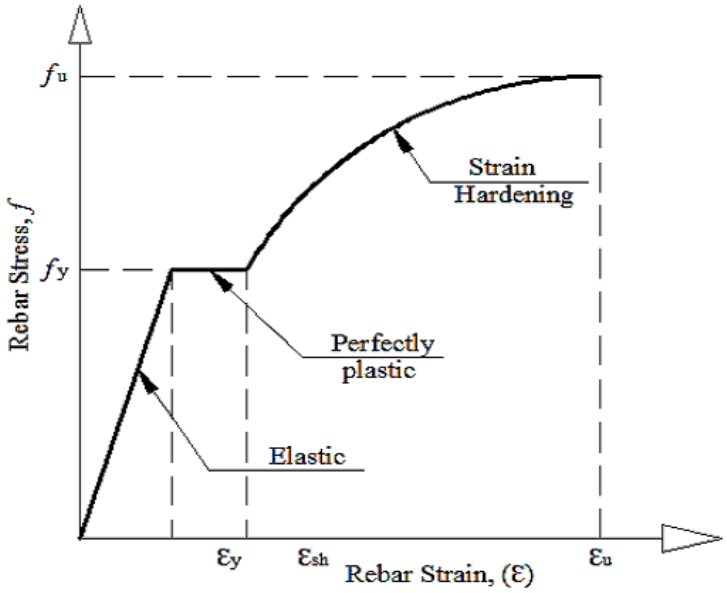

Figure 3.3**:** Rebar stress-strain curve (Mander et al, 1988)

3.3.2 Design load combinations

For seismic design to ES EN 1998:1-2015, determination of internal forces included a combination of gravity and seismic loads as shown below. For every structural element, the combination producing the greatest effects was used in the design.

$$DL + LL \quad 3.1$$

$$1.35DL + 1.5LL \quad .3.2$$

$$DL + 0.3LL \pm Eqx \pm 0.3Eqy \quad 3.3$$

$$DL + 0.3LL \pm Eqy \pm 0.3Eqx \quad 3.4$$

3.3.3 Seismic load parameters

Ground motion

Design ground accelerations of 0.15g was chosen for the design of low, medium and high ductility class considering the consequence associated with its collapse. Ground type C was assumed, corresponding to a deep deposits of dense or medium dense sand, gravel or stiff clay stratigraphic profile. Horizontal response spectrum Type 1 was used. Values of horizontal response spectrum used are shown in Table 3 ES EN 1998:1-2015.

Table 3.3: Values of horizontal response spectrum

Parameter	Value
Soil Class Factor (S)	1.15
Limits of Constant Spectral Acceleration Branch (TB) (sec)	0.2
Limits of Constant Spectral Acceleration Branch (TC) (sec)	0.6
Start of Constant Displacement Range of Spectrum (TD) (sec)	2

Table 3.4**:** Behavior factors used for the analysis.

Model type	Behavior factor
High ductility design	5.85
Medium ductility design	3.9
Low ductility design	1.5

3.3.4 Analysis verification and 2nd order effects

1. **Ultimate limit states**: For ultimate limit states verifications, Inter story drift sensitivity coefficient should be evaluated as follows.

   $\theta = \frac{P_{tot}.d_r}{V_{tot}.h} \le 0.10$, where θ is inter story drift sensitivity coefficient, P_{to} is total gravity load at each floor level, V_{tot} is story shear at the floor level, h is inter story height, and d_r is story drift

2. **Damage limit state:** The "damage limitation requirement" is considered to be satisfied, if story drift is limited.

   $d_r V \le (0.005-0.01)h$, where V is the reduction coefficient

Table 3.5**:** Analysis output and drift sensitivity check in y direction

	Story	Direction	Drift	P (kN)	V(kN)	θ	Check	
							ULS	SLS
DCL	Story6	Y	0.002362	3923.042	864.1442	0.010723	ok	ok
	Story5	Y	0.003964	7846.084	1500.849	0.020723	ok	ok
	Story4	Y	0.005248	11769.13	2037.376	0.030316	ok	ok
	Story3	Y	0.006241	15692.17	2452.378	0.039935	ok	ok
	Story2	Y	0.006755	19615.21	2729.046	0.048552	ok	ok
	Story1	Y	0.004768	23538.25	2867.38	0.03914	ok	ok
DCM	Story6	Y	0.001294	3923.042	288.992	0.01756594	ok	ok
	Story5	Y	0.00201	7846.084	470.9649	0.03348578	ok	ok
	Story4	Y	0.002583	11769.13	608.5948	0.04995058	ok	ok
	Story3	Y	0.003009	15692.17	732.702	0.06444331	ok	ok
	Story2	Y	0.003122	19615.21	815.4402	0.07509893	ok	ok
	Story1	Y	0.001932	23538.25	856.8093	0.05307587	ok	ok
DCH	Story6	Y	0.000898	3923.042	199.4912	0.01765938	ok	ok
	Story5	Y	0.001405	7846.084	328.0099	0.03360797	ok	ok
	Story4	Y	0.001818	11769.126	426.9563	0.05011349	ok	ok
	Story3	Y	0.002123	15692.168	514.023	0.06481125	ok	ok
	Story2	Y	0.0022	19615.21	572.0675	0.07543421	ok	ok
	Story1	Y	0.001358	23538.252	601.0898	0.05317832	ok	ok

3.3.5 Design results

Using the data given, ETABS was used to perform a response spectrum analysis on the structures. Design of structural members to the various loads was carried out using ETABS with the load combination that produces the maximum internal forces.

In the design of the buildings, the following points have been checked and kept in the required limit as per ES EN 1998:1-2015.

1. For (ULS) verifications, inter story drift has been checked and presented in Tables 3.5.
2. In frames fulfillment of strong column / weak beam capacity design rule, with over strength factor greater than 1.3.
3. Capacity design of members and joints in shear is done using ETABS vs 2016.2.1.
4. Plastic hinge regions are detailed on the basis of curvature ductility factor that corresponds to different ductility classes.

Sample reinforcement detail for beam and column

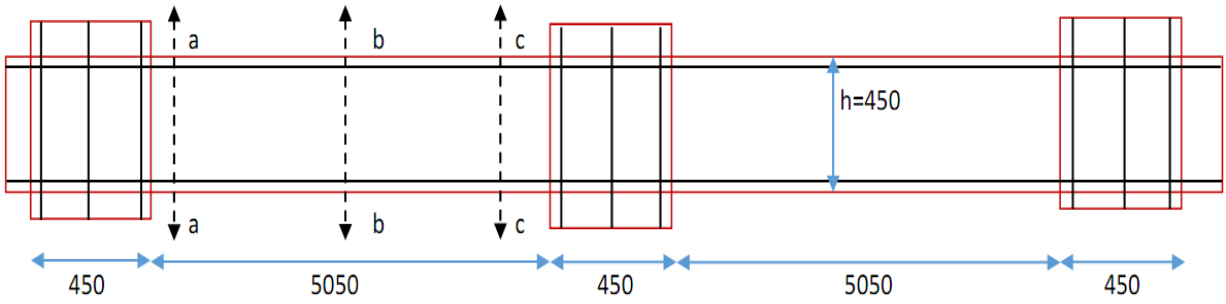

Figure 3.4: Beam detailing

In seismic design since seismic lateral force increases from DCH to DCL, building designed with DCL will have higher longitudinal reinforcement ratio when compare with DCH and DCM. In other hand, DCH will have higher transverse reinforcement compare with DCL and DCM which gives better confinement leading to higher rotation capacity.

Table 3.6: Sample beam detailing for Axis 1 first floor

Model		Length (mm)	Longitudinal reinforcement				Transverse reinforcement	
			a-a section		b-b section		In critical region	Outside critical region
			Top	Bottom	Top	Bottom		
High ductility design	B16	5050	3Φ16	2Φ16	2Φ16	2Φ16	10Φ C/C 80	10Φ C/C 110
	B17	5050	2Φ16&1Φ20	2Φ16	2Φ16&1Φ20	2Φ16	10Φ C/C 80	10Φ C/C 110
	B18	5050	2Φ16&1Φ20	2Φ16	2Φ16&1Φ20	2Φ16	10Φ C/C 80	10Φ C/C 170
	B19	5050	3Φ16	2Φ16	2Φ16	2Φ16	10Φ C/C 80	10Φ C/C 170
Medium ductility design	B16	5050	3Φ20	3Φ14	2Φ20	3Φ14	8Φ C/C 110	8Φ C/C 150
	B17	5050	2Φ14&2Φ20	2Φ16&1Φ14	2Φ20	2Φ16&1Φ14	8Φ C/C 110	8Φ C/C 150
	B18	5050	2Φ16&2Φ20	2Φ16&2Φ14	2Φ20	2Φ16&2Φ14	8Φ C/C 110	8Φ C/C 230
	B19	5050	2Φ16&2Φ20	2Φ16&2Φ14	2Φ20	2Φ16&2Φ14	8Φ C/C 110	8Φ C/C 230
Low ductility design	B16	5050	6Φ20	2Φ20&2Φ16	6Φ20	2Φ20&2Φ16	8Φ C/C 280	8Φ C/C 280
	B17	5050	6Φ20	4Φ16	3Φ20	4Φ16	8Φ C/C 280	8Φ C/C 290
	B18	5050	6Φ20	3Φ20	3Φ20	3Φ20	8Φ C/C 280	8Φ C/C 280
	B19	5050	6Φ20	2Φ20&2Φ16	3Φ20	2Φ20&2Φ16	8Φ C/C 280	8Φ C/C 280

B stands for the beams shown in Fig 3.1

Table 3.7: Bottom story column reinforcement

Model	size	Longitudinal reinforcement	Transverse reinforcement	
			In critical region	Outside critical region
Medium ductility design	450×450	8Φ20	8Φ C/C 110	8Φ C/C 280
High ductility design	450×450	4Φ20&4Φ16	8Φ C/C 90	8Φ C/C 110
Low ductility design	450×450	4Φ20&4Φ24	8Φ C/C 280	8Φ C/C 280

CHAPTER 4 PROGRESSIVE COLLAPSE ANALYSIS

4.1 Nonlinear Static (Pushdown) Analysis

Progressive collapse may be analyzed with linear static, nonlinear static or nonlinear dynamic procedures (GSA, 2013). Each analysis method possesses some advantages and disadvantages with respect to accuracy and running time. The GSA guidelines specify four column loss scenarios (Cases) in the assessment of the progressive collapse of a building. Each of the four buildings for this study was analyzed with the nonlinear static (pushdown) method. And it used for the four different column loss Cases. Figure 4.1 illustrates the positions of the removed columns in the various column loss cases, which are:

Case 1: An exterior column near the middle of the long side of the building

Case 2: An exterior column near the middle of the short side of the building

Case 3: A column located at the corner of the building

Case 4: A column interior to the perimeter

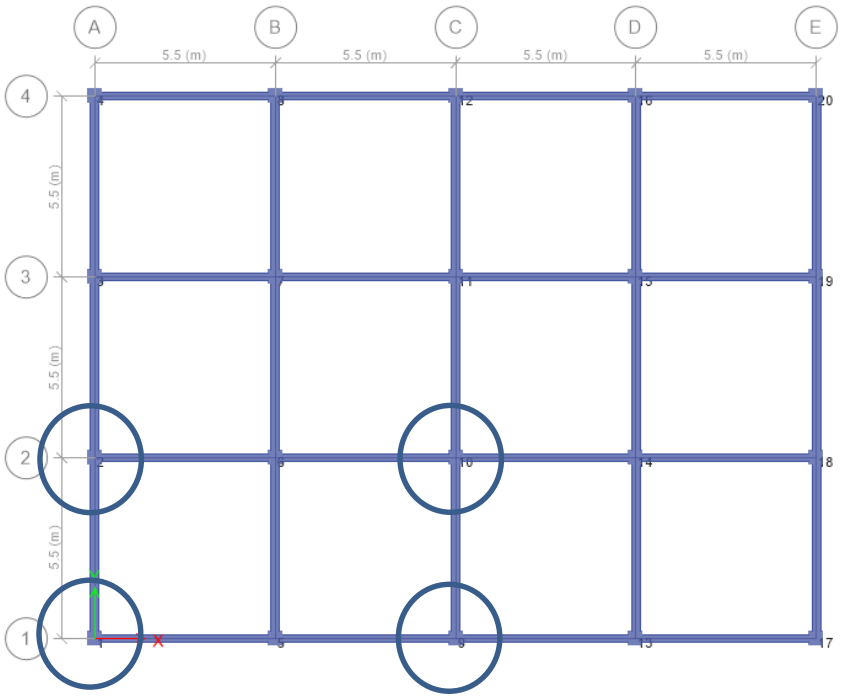

Figure 4.1: Location of column removal

The Nonlinear Static procedure involves a stepwise increase of vertical loads, until a maximum amplified load of $\Omega_N \left[1.2D+(0.5L)\right]$ is reached or the structure collapses. This method has the advantage of accounting for nonlinear effect without sophisticated hysteresis material model and time-consuming time-history analysis. In this study, the displacement controlled pushdown analysis was carried out by increasing the applied load to increase the vertical displacement at the location of the removed column until collapse. By this, the structure's resistance against such deformation is investigated.

4.1.1 Plastic hinge properties for seismically design buildings

For the nonlinear alternate path method, plastic hinges are allowed to form along the members. These hinges are based on maximum moment values calculated using the section design property employed to model the reinforced concrete structural elements. Recent experimental studies and numerical studies had shown that the collapse of RC framed structures is governed by the flexural failure mode of beam elements. Therefore, only this failure mode is investigated herein and not the shear failure. Therefore, only moment M3 is considered to cause a plastic hinge in flexural members and the axial-moment interaction (P-M2-M3) is considered to cause a plastic hinge in a column with relative hinge location of 0.05 and 0.95 for both beam and column.

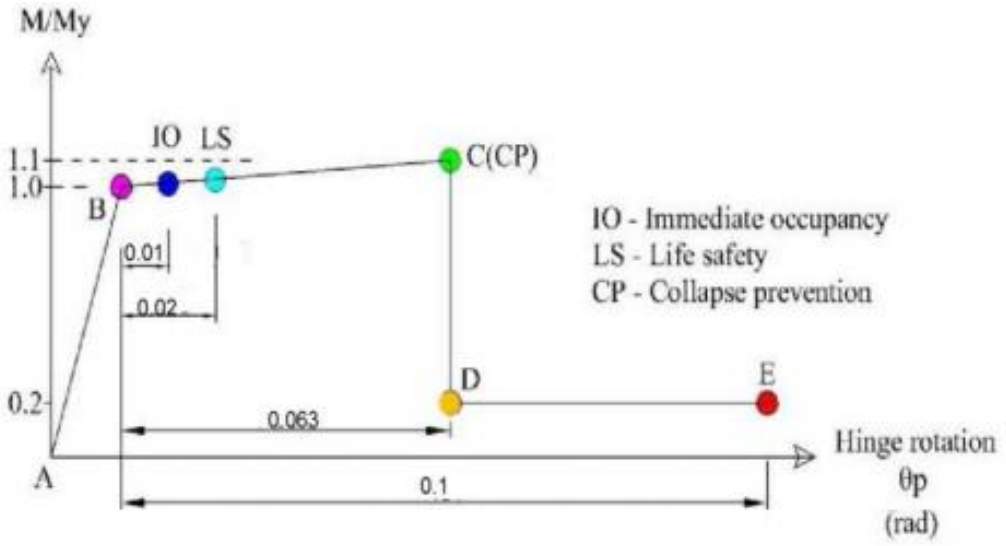

Figure 4.2: Plastic hinge property as per GSA guidelines

To create moment rotation curve for the plastic hinges of seismically designed (robust) structure the following points were consider.

- θ_y is 0, since yield rotation is distributed over the length of span.
- θ_u represents the collapse point correspond to point C. It is calculated from moment curvature relationship generated from SAP2000 section designer.
- Point C on the curve represents the collapse point and was assigned a rotation which is calculated from moment curvature relationship generated from SAP2000. The slope from point B to C was taken as 10% of the elastic slope. This accounts for strain hardening; the seismic code ASCE 41(2006) indicates that the slope should be taken as a small percentage between 0% and 10%. Point D corresponds to the residual strength 0.2 of the ultimate strength. Point E the failure limit is recommended by GSA (2013) guideline.

4.1.2 Rotational limit

The maximum allowable plastic rotations and ductility for a reinforced concrete structure according to GSA (2013) given in the Table 2.3.

Detailed hinge properties for different performance levels as specified by FEMA 356 (2000) were used to monitor the performance of the structures at different stages. The performance levels used include Immediate Occupancy (IO), Life Safety (LS), and Collapse Prevention (CP). These performance levels were used to monitor the state of the buildings as loads was applied.

4.1.3 Plastic hinge properties for deficient detailing

A deficient structure is structure designed using provisions that did not have the stringent detailing and structural integrity requirements of current codes. The effect of a short embedment length of the bottom flexural reinforcement at a connection is considered. The cracking moment is assumed to be the maximum moment capacity for the positive bending at a connection to reflect a short embedment length as shown in the Figure 4.3.

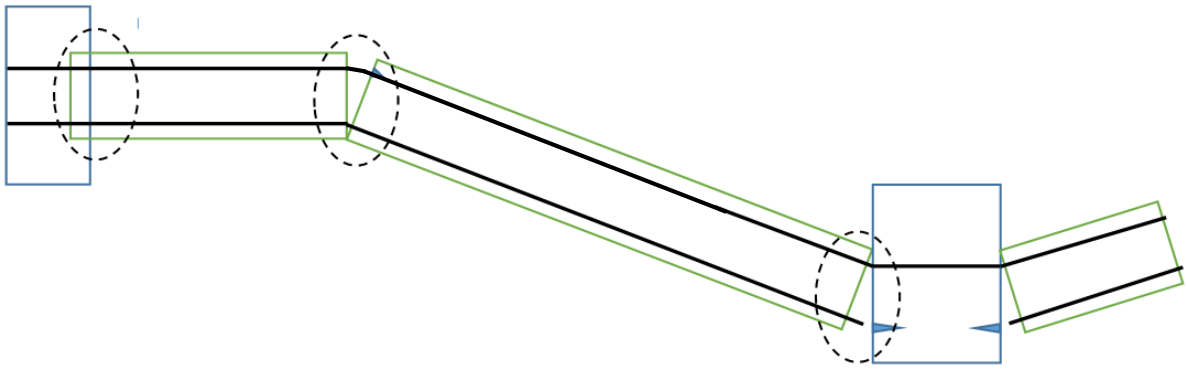

Figure 4.3**:** Typical frame with deficient reinforced beam and location of plastic hinge

The development length or anchorage of the bottom longitudinal reinforcement at the connection in to the column is inadequate to allow the reinforcement to yield during progressive collapse which allow moment reversal at beam column joining. This deficiency is reflected in calculating positive moment capacity at these locations. Therefore, cracking moment (Mcr) was considered as a maximum capacity that a concrete section can carry when a column is removed. The plastic rotation limit for a beam with the insufficient development length is 0.003 in GSA (2013).

4.2 Results and Discussion

4.2.1 Axial load redistribution

The transfer of load to the adjacent columns through the beams generated greater bending moments in the beams than before the loss of the column, as shown in Figure 4.4. For illustration of moment interaction of beams with columns, Figure 4.4 shows the moment diagrams for the frame on Axis 1 before and after the removal of column (Case 1). Not only did the bending moments increase, there was also a change in direction at the joints connection of removed column. For example, in beam beside remove column, the moment at the far side of beam increased from -37.8.0kNm to -199.26kNm, while the end connected to removed column changed from -36.3kNm to +150.63kNm (Figure 4.4).

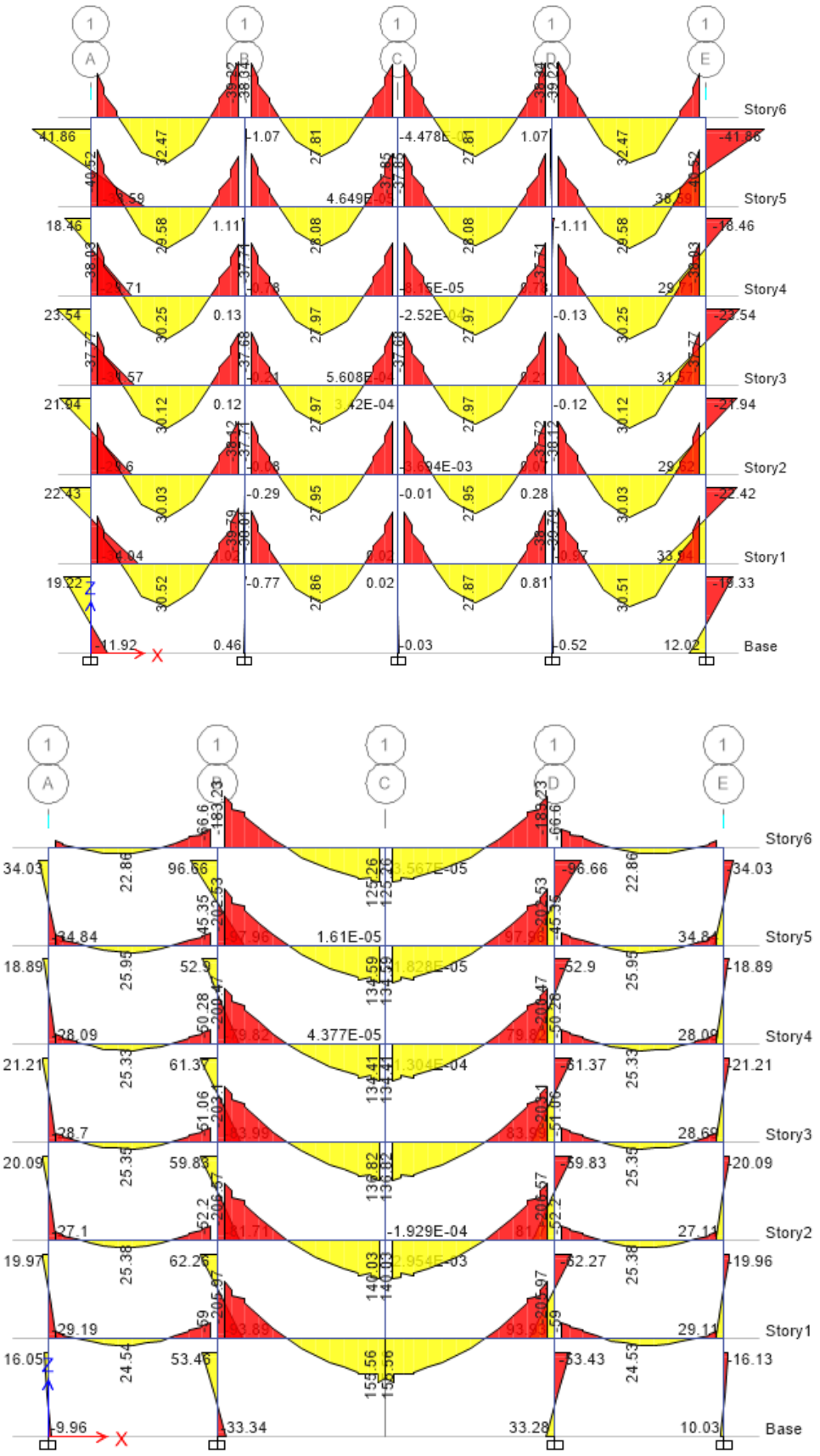

Figure 4.4: Bending moments (kNm) (a) before and (b) after loss of column (Case 1)

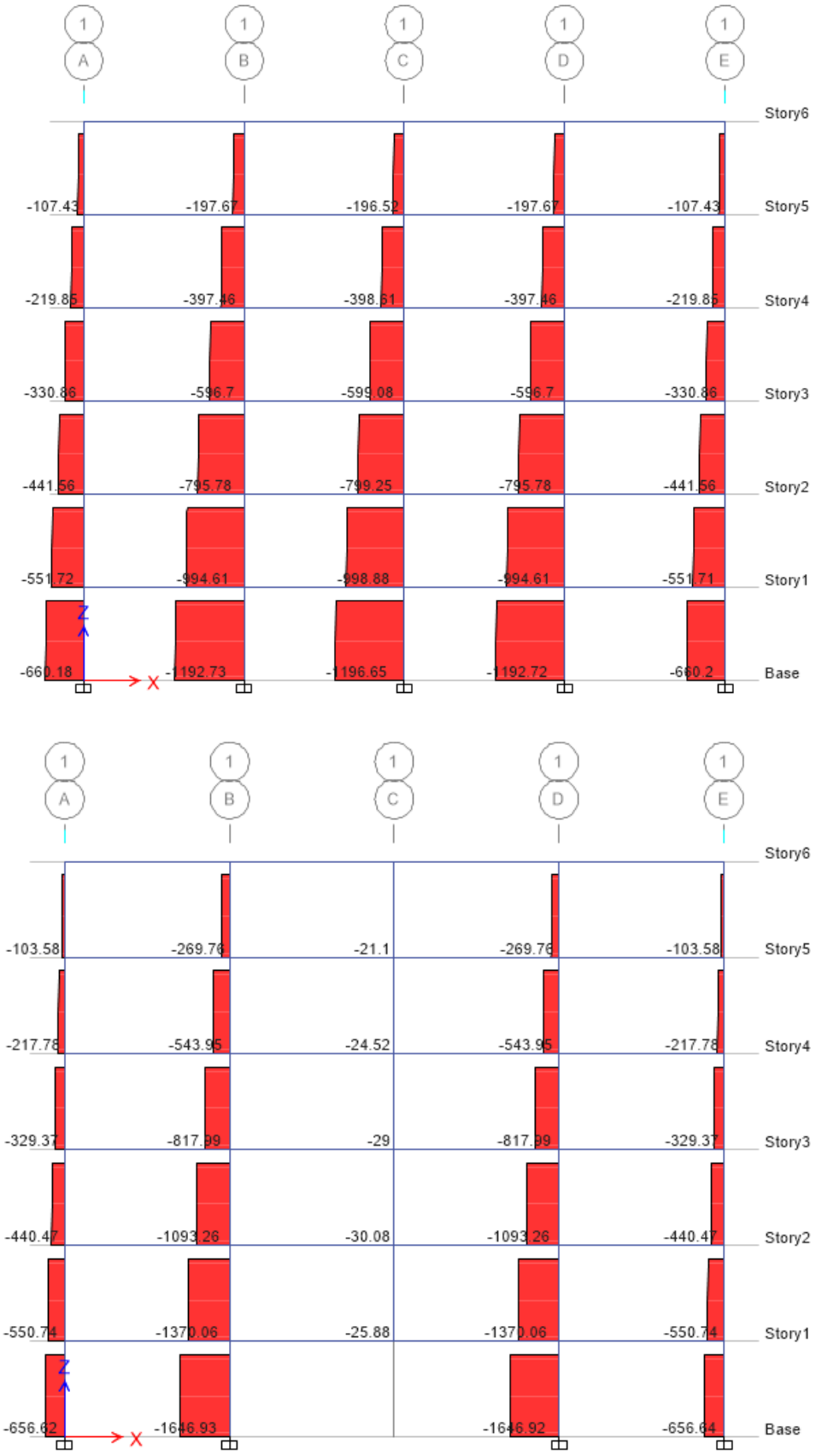

Figure 4.5: Axial force (kNm) (a) before and (b) after loss of column (Case 1)

After column C9 was removed (Case 1), the axial load it carried was transferred to the other columns on the ground floor through beams B7, B17 and B18 (see Figure 3.1) by Vierendeel action. Column C5 and C13 carried a final axial load of 1646.92kN giving it the highest percentage of the axial load of column C9 as 38.08% and columns C10 had 18.21%. The values of permanent axial loads in the rest of the columns after the removal of column C9 were found to be lower than the values before the removal. This was caused by the permanent side-sway of the structure towards Axis 1 after the column removed, as shown in Figure 4.6. Table 4.1-4.4 show the axial load percentages redistributed to the other ground floor columns after the four column removal cases. The axial load transfer to the ground columns before and after the removal of critical columns are listed in the Appendix D.

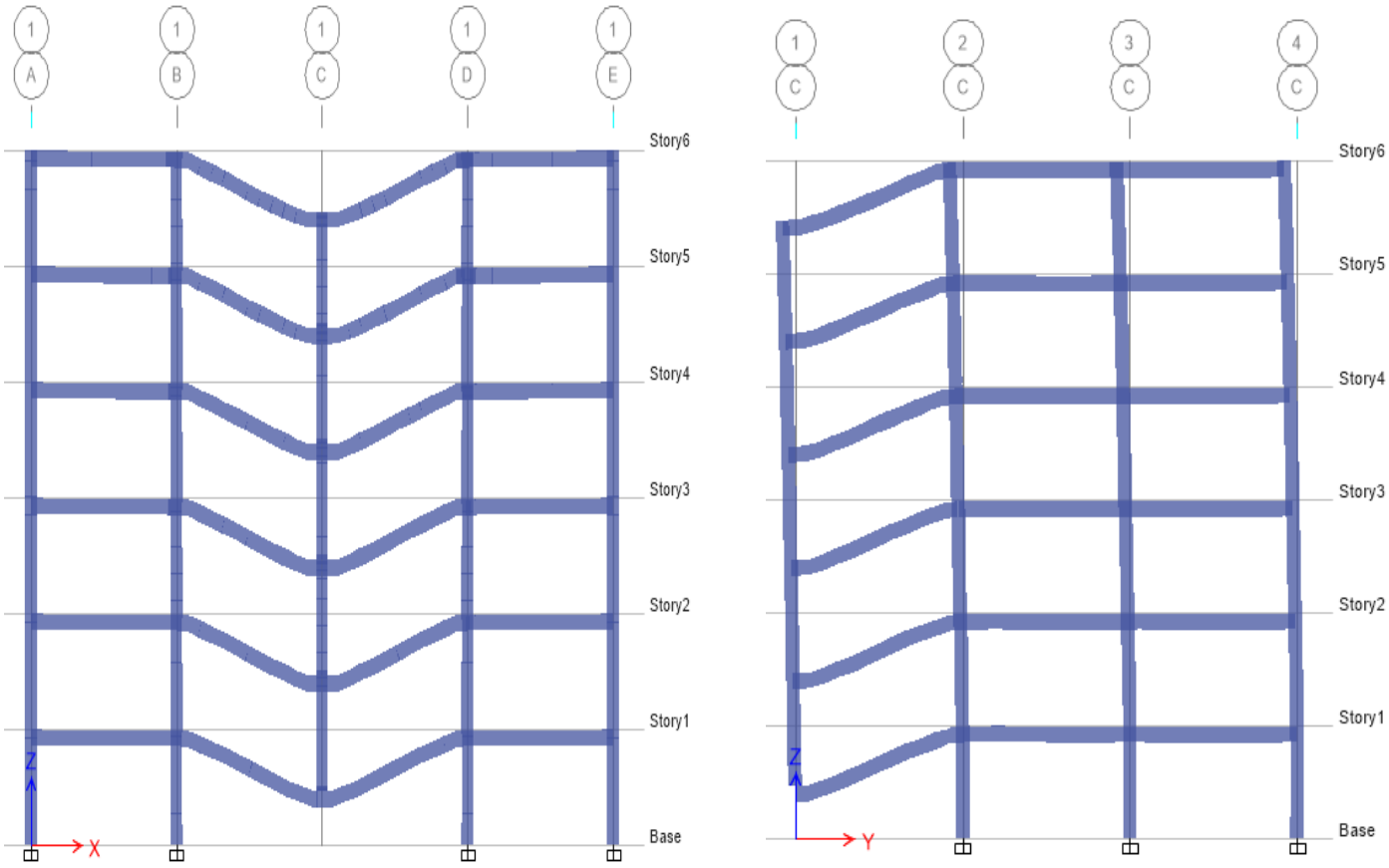

Figure 4.6**:** Deformed shape of frame after loss of column (Case 1) (a) Axis 1 (b) Axis C

Table 4.1: Percentage redistribution of axial loads in Case 1

Axis	A	B	C	D	E
1	-0.54	**38.08**	Removed	**38.08**	-0.54
2	-0.29	0.49	**18.21**	0.49	-0.29
3	0.15	-0.01	-1.21	-0.01	0.15
4	-3.49	-2.00	-1.95	-2.00	-3.49

Table 4.2**:** Percentage redistribution of axial loads in Case 2

Axis	A	B	C	D	E
1	**62.39**	0.21	-0.29	0.40	-3.18
2	Removed	**17.88**	-1.24	0.12	-2.12
3	**37.73**	0.48	-0.09	0.08	-1.66
4	-0.13	0.27	0.15	-0.16	-3.37

Table 4.3: Percentage redistribution of axial loads in Case 3

Axis	A	B	C	D	E
1	Removed	**32.12**	-0.26	1.65	-0.09
2	**32.10**	0.28	-0.15	0.01	-1.64
3	-0.06	-0.07	-0.08	0.13	-1.75
4	-0.26	-2.18	-1.81	-1.38	-5.80

Table 4.4: Percentage redistribution of axial loads in Case 4

Axis	A	B	C	D	E
1	-0.70	1.18	**43.40**	1.18	-0.69
2	-3.07	**25.72**	Removed	**25.72**	-3.07
3	-0.23	0.87	**26.27**	0.87	-0.23
4	0.36	-0.03	-29.2	-0.05	0.36

4.2.2 Pushdown result

The nonlinear static progressive analysis also known as the pushdown analysis was carried out by gradually increasing the gravity loads to increase the vertical displacement at the location of the removed column and the plastic rotations in the members until the structure collapses. The relationship between the vertical displacement at the location of the removed column and the increasing loads was evaluated in each case of column removal. The development of plastic hinges in the beams and columns were monitored for the collapse assessment of the structures.

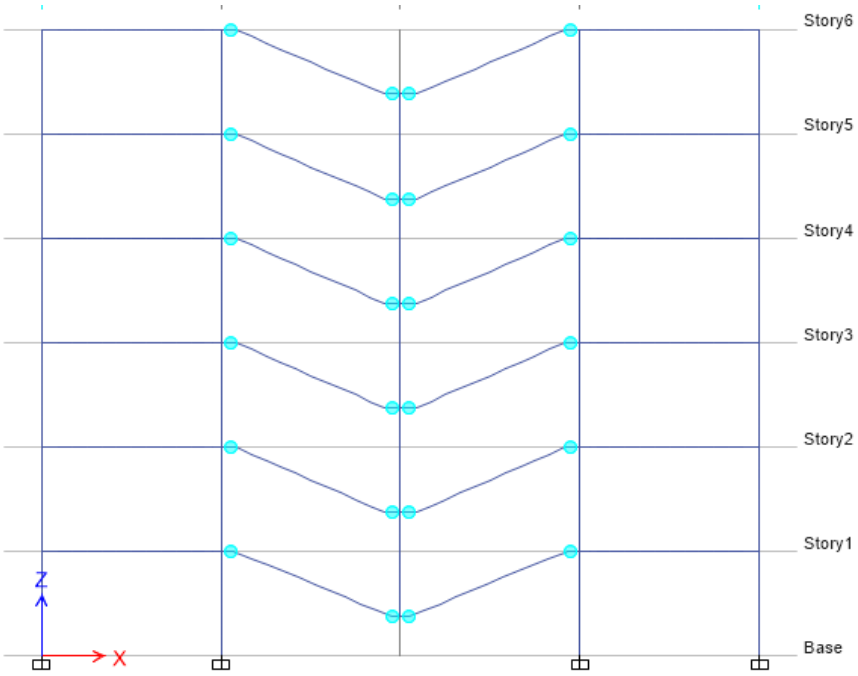

Figure 4.7: Plastic hinge formation for high ductility design, Axis 1 (Case 1)

The vertical displacement and the corresponding normalized vertical loads for all the buildings are plotted in Figures 4.8 – 4.11 for the various column loss scenarios. Different loading areas are supported by the various removed columns; hence, the total vertical loads supported by the columns are different. Therefore, the ratios of the applied vertical loads at each step to the load of $\Omega_N \left[1.2D+0.5L\right]$, which is known as load factor, were used in the graph as the loading parameter and plotted on the vertical axis. The horizontal axis represents the displacements of the joint above the removed column. This graph is called pushdown curve which analogues to the pushover curve. The collapse resistance of a building was as its ability to carry the ultimate load of $\Omega_N \left[1.2D+0.5L\right]$ before collapse.

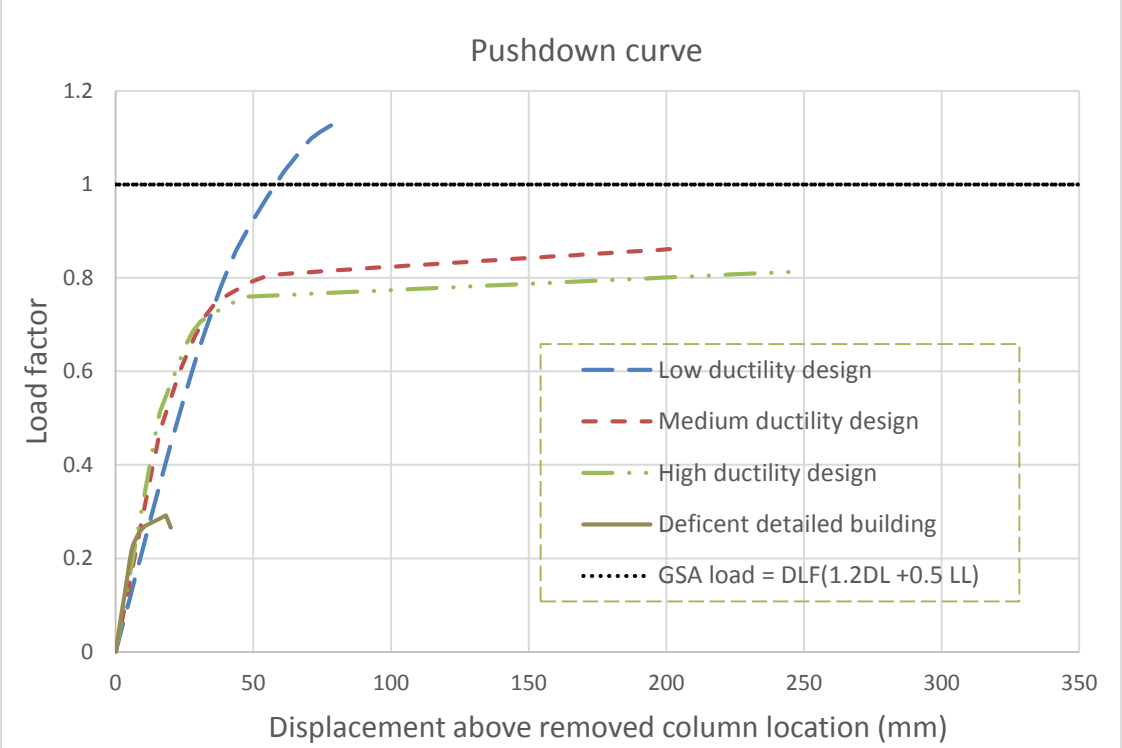

Figure 4.8**:** Pushdown curve for Case 1

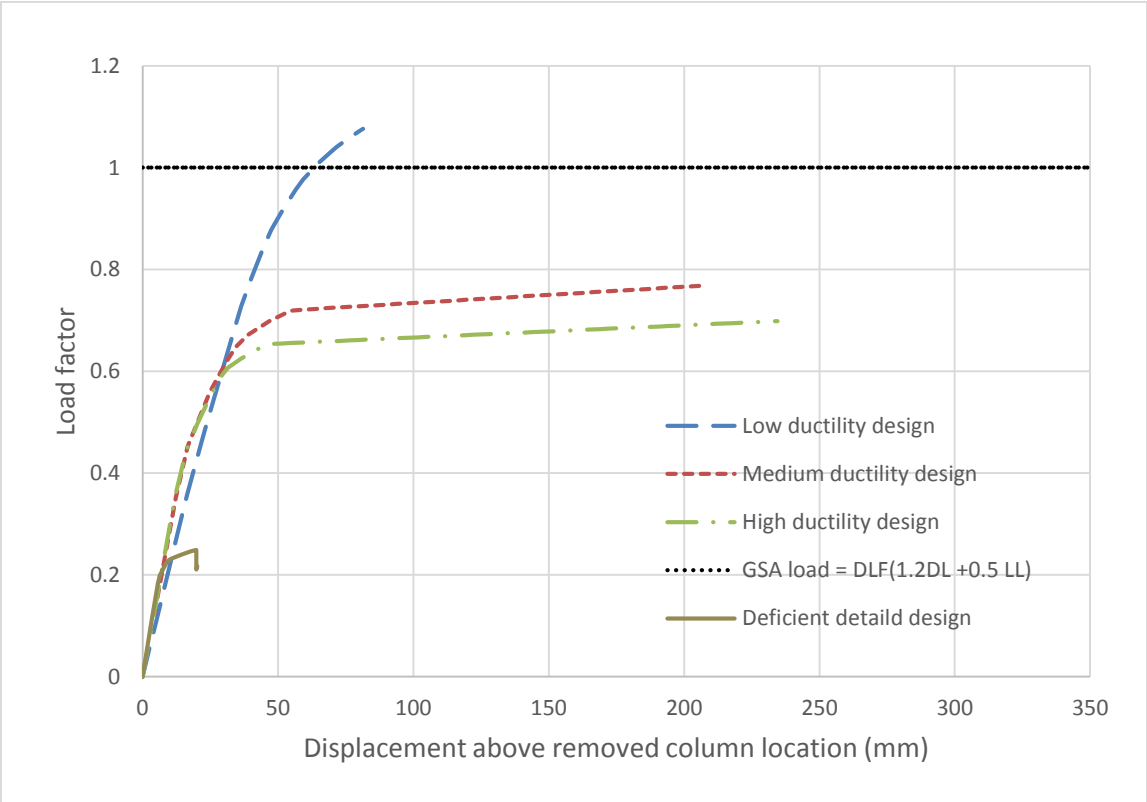

Figure 4.9: Pushdown curve for Case 2

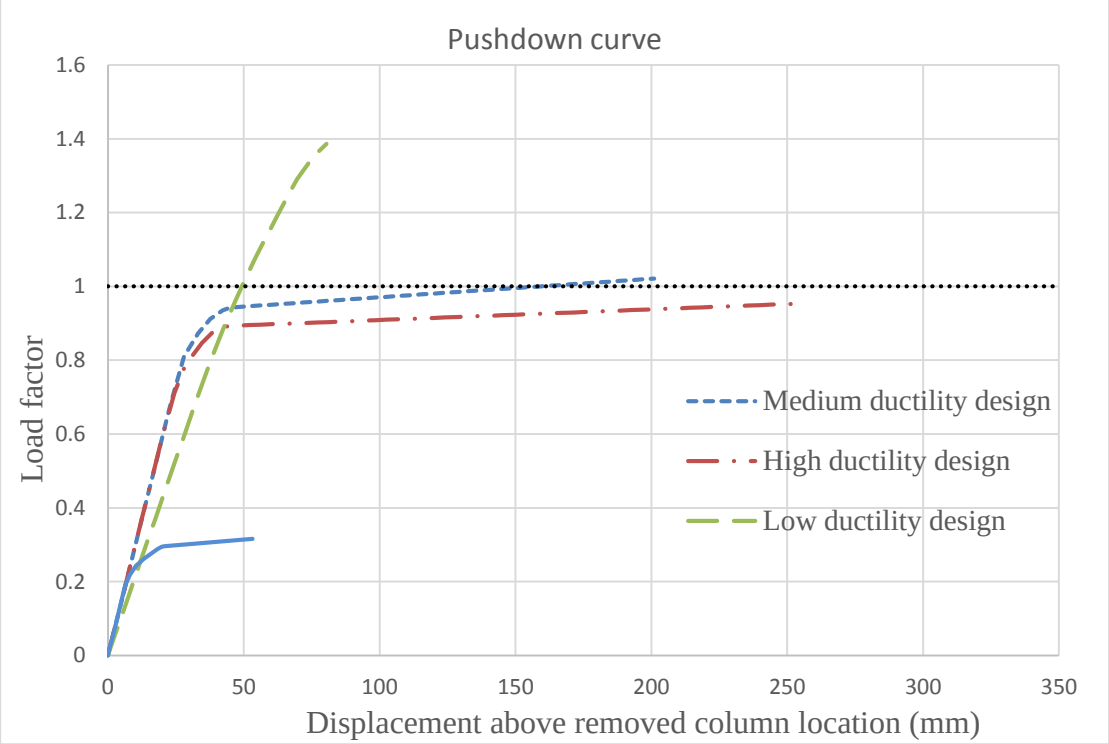

Figure 4.10**:** Pushdown curve for Case 3

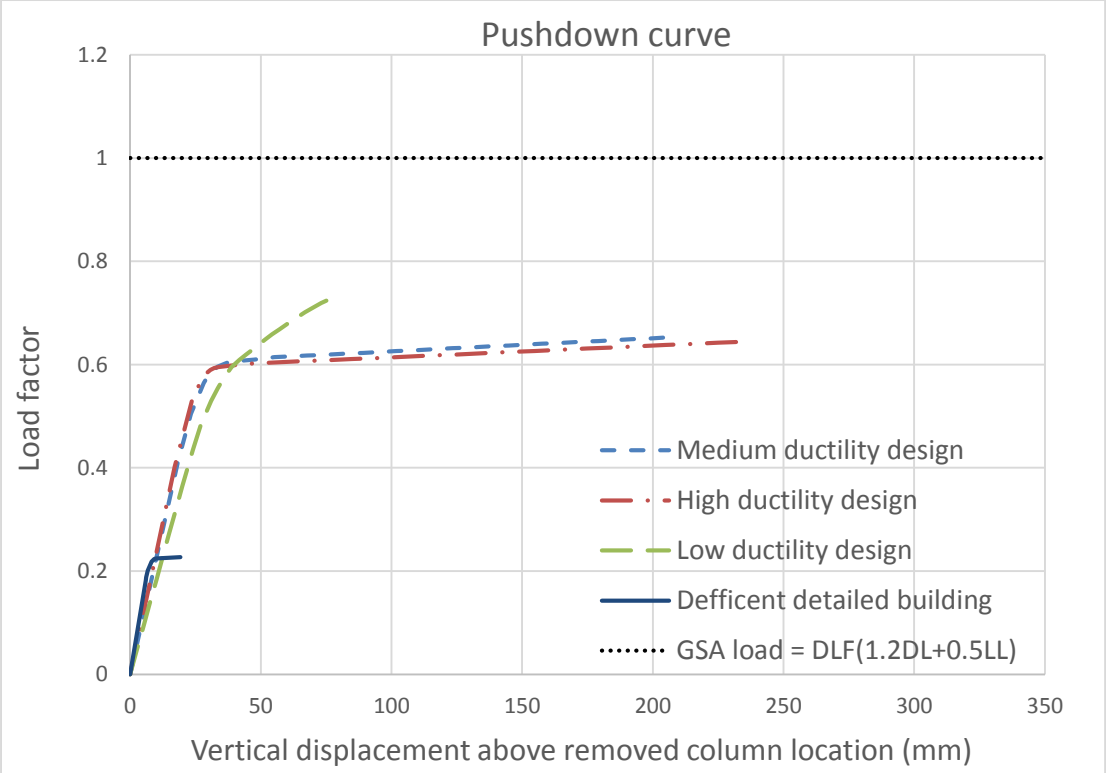

Figure 4.11**:** Pushdown curve for Case 4

Table 4.5: Maximum load factors

Model	Case 1	Case 2	Case 3	Case 4
High ductility design	0.814	0.698	0.953	0.644
Medium ductility design	0.862	0.769	1.021	0.652
Low ductility design	1.13	1.076	1.386	0.733
Deficient detailed design	0.266	0.217	0.316	0.210

Generally in pushdown curve, if the curves attain a value of load factor 1 and above it means that, the remaining structure is capable to carry the additional induced progressive collapse load $\left(\Omega_N \left[1.2D+0.5L\right]\right)$, or else the building will fail before the standard GSA loading is attained (Figures 4.8- 4.11).

When a column was removed from near the middle of the long side (Case 1) and short side (Case 2) of the buildings, all the models except low ductility design weren't resilient to progressive collapse in the GSA nonlinear static analyses Thus, collapse did occur under the full gravity loads.

When a corner column was removed (Case 3), low and medium ductility design were resilient to progressive collapse with maximum load factor 1.386 and 1.021 respectively.

When internal column was removed (Case 4) all the model was exposed to progressive collapse according to GSA 2013 guidance and Case 4 happens to be most vulnerable condition of all cases with lower load factor.

From the pushdown curve (Figures 4.8- 4.11), it is observed that the structures resisted progressive collapse by two main mechanisms. These are strength and ductility. Low ductility class models had an advantage of high strength and therefore had higher yield loads and ultimately higher collapse loads. On the other hand high ductility models yielded at lower loads, but were able to undergo relatively higher deformations, enabling them to absorb more energy and try to prevent collapse, even if it had lowest load factor value.

It is also observed from GSA analyses that the vulnerability of a structure to collapse was highest when an interior column is lost (Case 4). The buildings had resistance when corner column loss. Mostly, Case 3 had marginally higher load factors, implying that the structures were found to be most resilient when a column is lost from a corner of the building.

4.2.3 Plastic hinges rotations

The formation of plastic hinges in the beams at a loading level of $\Omega_N \left[1.2D + 0.5L\right]$ was monitored according to the GSA guidance. It is observed that for all models, plastic hinges were developed only in the beams but none in columns. The plastic rotations of hinges at the ends of the beams connected to the removed column were always lower than the other ends of the beams connected on top of the intact columns.

When a column was removed from the long side of the buildings (Case 1) plastic hinges developed in all models. Except deficient design, all models remained in the life safety performance level. Deficient detailed design responded at the collapse prevention performance level. Significant structural damage is expected with some margin against collapse remaining. Collapse was observed in deficient detailed design model, since it exceeded the rotation limit for beams controlled by inadequate development or splicing along the span (0.003 radians) (see Table 2.1). On the other hand, seismically designed building, which is controlled by beam flexural failure, did not reach the rotation limit provided by the GSA 2013 guideline, which allowed beam rotation to 0.063 radians.

Table 4.6: Maximum plastic hinge rotations (radians)

Model	Case 1	Case 2	Case 3	Case 4
High ductility design	0.0495	0.0464	0.0500	0.0466
Medium ductility design	0.0403	0.0413	0.0398	0.0405
Low ductility design	0.0159	0.0161	0.0159	0.0158
Deficient detailed design	0.0039	0.0037	0.0097	0.0038

Similarly Case 2, Case 3, and Case 4 plastic hinges developed in all model like Case 1 except deficient design all models remained in the life safety performance level. Deficient detailed design responded at the collapse prevention performance level. Collapse was observed in deficient detailed design model since it exceeded the rotation limit for beams controlled by inadequate development or splicing along the span (0.003 radians). Seismically designed building, which is controlled by beam flexural failure, allowed beam rotation to 0.063 radians based on GSA 2013.

The maximum plastic rotations required for nonlinear analysis were found to vary according to the seismic design parameters. The average plastic hinge rotations calculated were 0.0466, 0.0405 and 0.0167 for high, medium and low ductility classes respectively. It confirm that plastic hinge rotations for progressive collapse resistance increase with design ductility class.

4.2.4 Effects of structural deficiencies (poor detailing)

When a critical column was removed, structures with deficiencies had difficulty in transferring applied loads to alternate load paths due to lack of strength and ductility. If sufficient rotational capacities were provided by adjacent components, they would be able to transfer load from deficient components. Although plastic hinges in a robust structure were developed, hinges in beams and columns had sufficient rotational capacities to carry additional loads, and alternate load paths were well established.

By comparing seismically designed (robust structure) and deficient structure, the importance of structural integrity was demonstrated. A robust with good detailing exhibited more ductile behavior and larger load-carrying capacity than a deficient structure as predicted.

CHAPTER 5 ANALATICAL STUDY

During progressive collapse, beams adjacent to failed column faced large amount of bending moment demand as seen in the previous chapter. This demand largely resisted by compressive arch action and catenary action other than flexural action. Therefore, in this chapter effect of seismic design provision level on the development of CAA and CA will be studied.

5.1 Introduction

Flexure occur in reinforced concrete slab or beam member under loading, as a result of the great difference between the tensile and compressive strengths of concrete, the member deflects and the concrete on the tensile face cracks, causing an upward migration of the neutral axis level and resulting in an outward expansion of the member at the supports. If the tendency to expand is restrained by some stiff boundary elements, the structural response due to these in-plane compressive in-plane forces will be developed in the slab and beam. Axial forces is referred to as arching action in beam members (Figure 5.1).

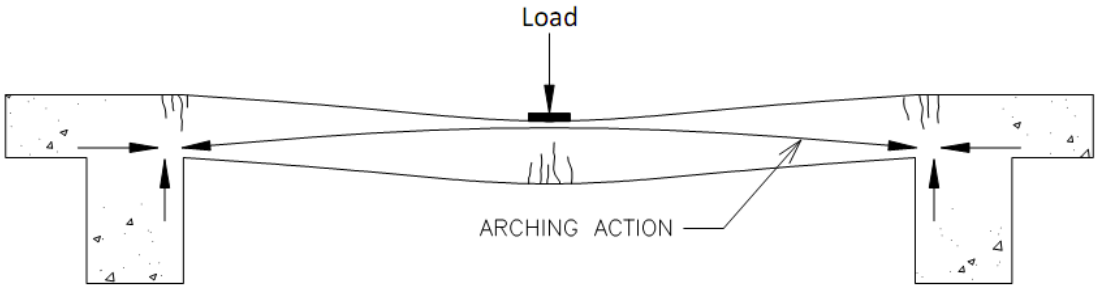

Figure 5.1 Arching action

Park (1964) depicted the influence of lateral restraint in the load-central deflection relationship of a uniformly loaded reinforced concrete slab as the curve shown in Figure 5.2. As the load increases from A, the yield line pattern develops with the help of compressive membrane forces until the slab reaches its enhanced ultimate load at B. The induced compressive membrane force in the slab results in an enhancement of the flexural strength of the slab sections.

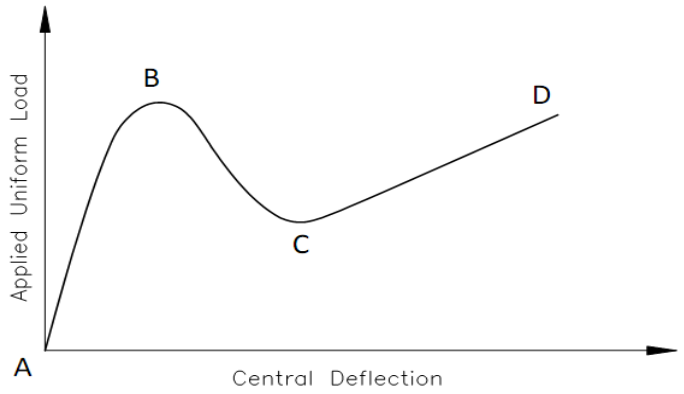

Figure 5.2: Load-deflection relationship for RC slabs with edges restrained against lateral movement (Park, 1964)

As the deflection increases beyond B, the load carried by the slab decreases rapidly because of a reduction in the compressive membrane force, caused by concrete crushing at critical regions. As C is approached, the membrane forces in the central region of the slab change from compression to tension. At more advanced stages of deflection beyond C, for slabs with rigid boundary conditions, the reinforcements can act as a tensile net and the slab continues to carry further load until at D the reinforcements begin to fracture. This second-stage behavior, from C to D, is called catenary action.

5.2 Simplified Methods of Modeling Compressive Arch Action (CAA)

Yu and Tan, 2014 modifying Park's model to predict CAA capacity of RC beams by incorporate the actual stress state of compression reinforcement, rotational and axial restraints. The detail development of the proposed model by Yu and Tan is explain below.

The proposed model

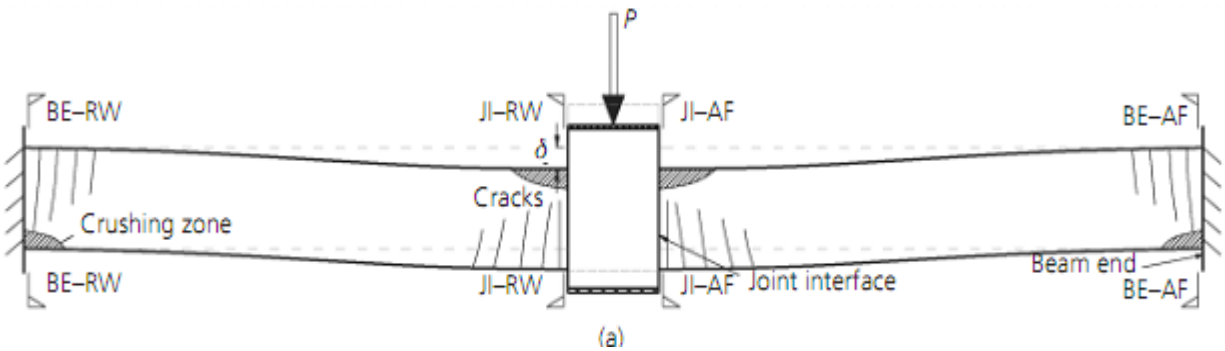

Figure 5.3: Beam-column sub-assemblage with a concentrated load (Yu and Tan, 2014)

Figure 5.3 shows that plastic hinges have occurred at the joint interfaces and the beam ends of an RC beam-column sub-assemblage with a concentrated load applied at the middle joint. Due to symmetry, the free body diagrams of a one-bay beam and the middle joint at CAA stage are shown in Figure 5.4(a) and (b), respectively.

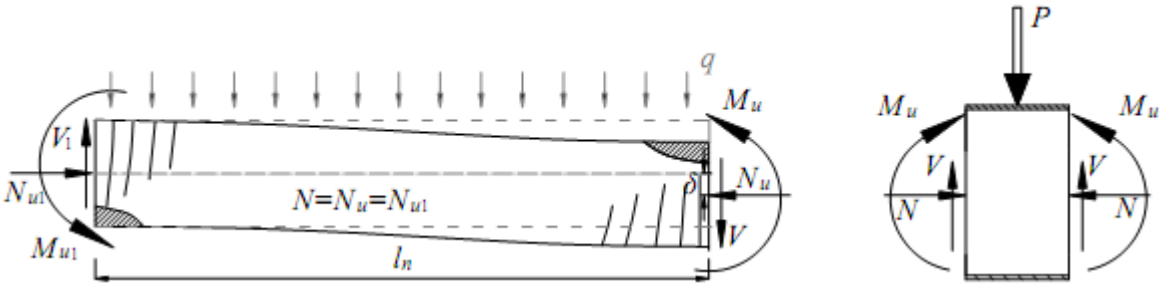

Figure 5.4 Free body diagrams of RC beam under CAA (a) One-bay beam (b) Middle joint (Yu and Tan, 2014)

Due to axial restraints at both ends of the beam, considerable axial compression is mobilized throughout the beam length. Provided that the resistance of the sub-assemblage based on shear failure is greater than that based on flexural failure, with consideration of $N-\delta$ effect, vertical resistance P is determined based on force equilibrium in the vertical direction at the middle joint as shown in Figure 5.4(b) and moment equilibrium in the one-bay beam as shown in Figure 5.4(a).

Axial force, $N_u = N_{ul} = N$ (5.1)

Shear force, $V_1 = V$ (5.2)

Applied load, $P = 2V$ (5.3)

By taking moment equilibrium about the end support in Figure 5.4(a):

$$VL = M_u + M_{ul} - N_u\delta \tag{5.4}$$

By substituting equations 1, 2 and 3 into equation 4, the load capacity can be obtained:

$$P = \frac{2(M_{u1} + M_u - N_u\delta - q\,l_n^2/2)}{l_n} \tag{5.5}$$

Where V is the shear force acting at the joint interfaces; M_u and M_{ul} are ultimate bending moments acting on the beam ends and the joint interfaces, respectively; N is the beam axial

compression; δ is the beam deflection at the middle joint; p is the self-weight or applied uniform loads on the beam; and l_n is the net span length of a one-bay beam.

Equation (5.5) suggests that to obtain the relationship of vertical resistance P and deflection δ of a sub-assemblage, the relationships of bending moment M and axial force N to δ should be determined first. Both M_u and M_{u1} can be estimated once N is known. Then the core of the proposed model is to obtain the relationship between N and δ. In the following subsections, N-δ relationship will be constructed through compatibility conditions and force equilibrium of sub-assemblages based on the following assumptions.

Assumptions of the proposed model

The proposed model applies only after plastic hinges have occurred at several critical sections, as shown in Figure 5.3. To compute the cross-sectional forces M and N, the conventional assumptions used in ACI 318-05 (ACI, 2005) are adopted. Namely

- a plane section remains plane
- At each critical section, compression concrete has attained its strength with an idealized equivalent rectangular stress block and an ultimate strain of 0.003 in the extreme compression fiber of concrete, tension reinforcement has yielded and concrete tensile strength is ignored.
- The restraints from surrounding structures are converted to equivalent axial and rotational restraints with linear elastic stiffness, and symmetrical at both end as shown in Figure 5.3.
- Axial shortening of beams is only induced by elastic axial compressive strains, which are uniform throughout the whole two-bay beam
- The material property of compressive steel reinforcement is elastic–perfectly-plastic, and the unloading slope after yielding equals the initial elastic modulus.

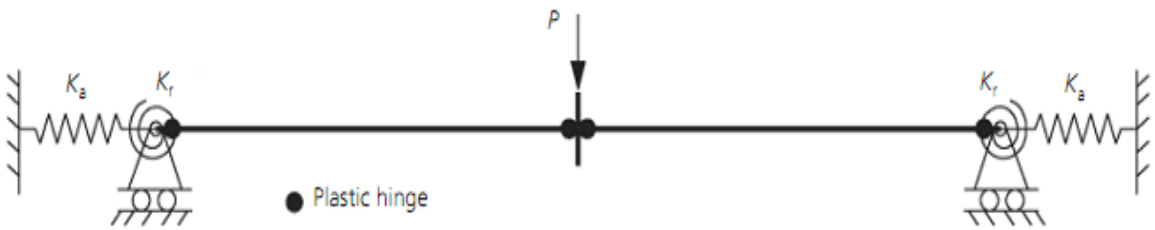

Figure 5.5 Equivalent boundary conditions for a two-bay beam (Yu and Tan, 2014)

Following the above assumptions, neutral axis depths at the beam ends and the middle joint interfaces, which are used to determine internal forces, will be linked to vertical deflection δ via compatibility conditions and force equilibrium.

Compatibility conditions

After the ultimate moments of resistance have been obtained at the beam ends and at the joint interfaces, due to symmetry, the deformation and the rotation of one-half sub-assemblage are exaggeratedly drawn in Figure 5.6. Due to mobilization of axial compression throughout the beam, the deformed beam causes horizontal expansion by an amount of $(t+t_0)$ and $0.5\varepsilon b_j$ at the lateral support and the middle joint interface, respectively. The term t is the small lateral deformation of the support and t_0 is the gap between the support and the beam end. The existence of t_0, caused by connection gaps, is found in the laboratory tests, so it is considered in the model. The term $0.5\varepsilon b_j$ represents small axial deformation of the middle joint, in which ε is axial strain throughout the middle joint equal to, $\varepsilon = N/E_c A$ according to assumption and b_j is the middle joint width.

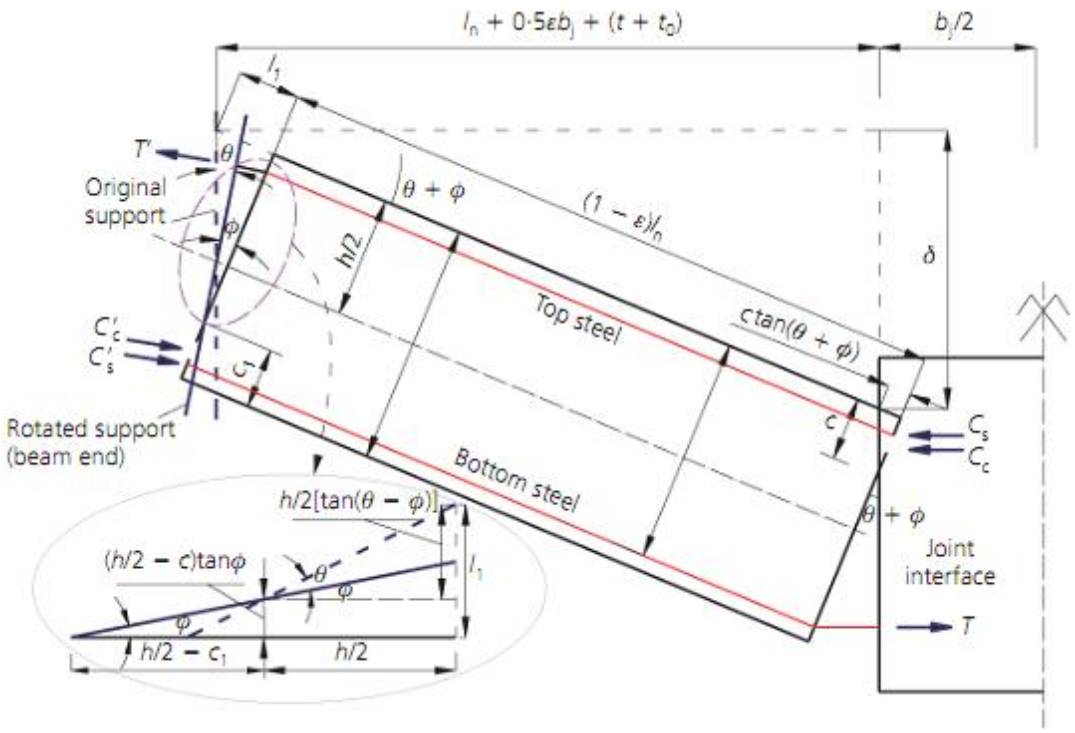

Figure 5.6: Compatibility conditions of beam-column sub-assemblage (Yu and Tan, 2014)

On the other hand, as shown in Figure 5.6, a large crack with a width of l_1 occurs at the beam end, and crushing of concrete with a length of $c\tan(\theta+\phi)$ happen at the middle joint interface, in which ∅ is the beam end rotation with respect to the rotated support and θ is the rotation of the lateral support at the beam end. Axial compression in the beam results in a contraction of εl_n along the axis of the deformed beam. Axial strain ε along the beam is assumed equal to the one in the middle joint, since the axial compression is constant throughout the whole sub-assemblage. As shown in Figure 5.6, the projection of the displaced beam segment onto the original beam configuration yields the compatibility equation.

$$\left[\mathrm{l}_n+0.5\varepsilon b_j+(t+t_0)\right]\sec(\phi+\theta)=l_1+(1-\varepsilon)\mathrm{l}_n-c\tan(\phi+\theta) \tag{5.6a}$$

Since the net span length of the single-bay beam is l_n and the middle joint width is b_j, the total net span length of the sub-assemblage is $l=2\mathrm{l}_n+b_j$. If the ratio l_n/l denoted as β, the joint width b_j can be expressed as $(1-2\beta)l$ and Eq. (5.6a) can be converted into:

$$\left[\beta l+0.5\varepsilon(1-2\beta)l+(t+t_0)\right]\sec(\phi+\theta)=l_1+(1-\varepsilon)\beta l-c\tan(\phi+\theta) \tag{5.6b}$$

According to geometric relationships at the beam end restrained by the external support crack width l_n at the beam end (i.e. the distance of the top fiber at the beam end to the original support) is given by:

$$l_1=\frac{h}{2}\tan(\varphi+\theta)+\left(\frac{h}{2}-c_1\right)\tan\phi \tag{5.7}$$

where h is the beam depth and c_1 is the neutral axis depth at the beam end.

Substituting Eq. (5.7) into Eq. (5.6b) and rearranging the equation to obtain the expression for the neutral axis depth c at the middle joint interface, the following equation is obtained.

$$c=\frac{h}{2}-\frac{0.5\varepsilon l+(t+t_0)}{\sin(\phi+\theta)}-(1-\varepsilon)\beta l\frac{2\sin^2\left[(\phi+\theta)/2\right]}{\sin(\phi+\theta)}+\left(\frac{h}{2}-c_1\right)\frac{\tan\phi}{\tan(\phi+\theta)} \tag{5.8}$$

Detailed simplification process for Eq. (5.8) is given in Appendix A.

Since the partial rotational restraint at the beam ends is assumed as a linear elastic spring with a stiffness K_r when the bending moment M_{ul} acts at the beam end, the corresponding rotation of the lateral support θ can be obtained.

$$\theta = M_{ul} / K_r \tag{5.9}$$

Moreover, axial strain ε of the beam segment and outward lateral displacement t of the linear elastic axial restraint at the beam end are determined by the induced beam axial compression N throughout the beam. Since all plastic deformations are concentrated at the middle joint interface and the beam end, the beam segment is assumed to deform elastically and uniformly. Therefore,

$$\varepsilon = \frac{N}{bhE_c} \tag{5.10}$$

$$t = \frac{N}{K_a} \tag{5.11}$$

where b is the beam width; E_c is the elastic modulus of concrete and K_a is the stiffness of axial restraints. Since ∅ and θ are small, the trigonometric functions in Eq. (5.8) can be replaced by equivalent infinitesimal mathematical terms. Also, the beam axial strain ε and the movements of the axial restraints $(t + t_o)$ are extremely small compared with l_n.

Therefore,

$$\sin\theta \approx \theta = \frac{M_{ul}}{K_r};$$

$$\sin(\phi+\theta) \approx 2\sin\left(\frac{\phi+\theta}{2}\right) \approx \phi+\theta = \frac{\delta}{l_n + 0.5\varepsilon b_j + (t+t_0)} = \frac{\delta}{l_n} = \frac{\delta}{\beta l}, and \phi = \frac{\delta}{\beta l} - \frac{M_{ul}}{K_r}$$

$$\tan(\phi+\theta) \approx \phi+\theta; \tan\phi = \phi$$

Substituting Eqs. (5.10) and (5.11) and the equivalent values of the trigonometric functions into Eq. (5.8) gives the following equation:

$$c = \frac{h}{2} - \frac{\delta}{2} - \frac{\beta l^2}{2\delta}\left(\frac{1}{bhE_c} + \frac{2}{lK_a}\right)N - \frac{\beta l t_0}{\delta} + \left(\frac{h}{2} - c_1\right)\left(1 - \frac{M_{ul}\beta l}{K_r \delta}\right) \tag{5.12}$$

where c and c_1 are the neutral axis depths at the middle joint interface and the beam end, respectively. Detailed simplification process to obtain Eq. (5.12) is given by Appendix A.

Eq. (5.12) suggests that c can be expressed as a function of two variables c_1 and δ as both N and M_{ul} can also be determined by c_1, which will be explained later. Thus, for a given middle joint vertical displacement δ, c becomes a function of a single variable c_1. To solve two unknowns' c and c_1, another equation correlating them can be obtained via equilibrium condition.

Equilibrium condition

When a beam is under CAA, rotations of beam sections are very small, so that there is no appreciable discrepancy between horizontal reaction forces and axial forces throughout the beam (Yu and Tan 2013). Therefore, the axial forces acting at the beam ends (N_{ul}) and the joint interfaces (N_u) are equal. The magnitudes of N_{ul} and N_u are denoted as N.

$$N_u = N_{ul} = N \tag{5.13}$$

Based on assumptions the stress and strain distributions as well as internal force components at a beam section are shown in Figure 5.7. Both M and N are calculated with respect to the middle-depth axis of a beam section.

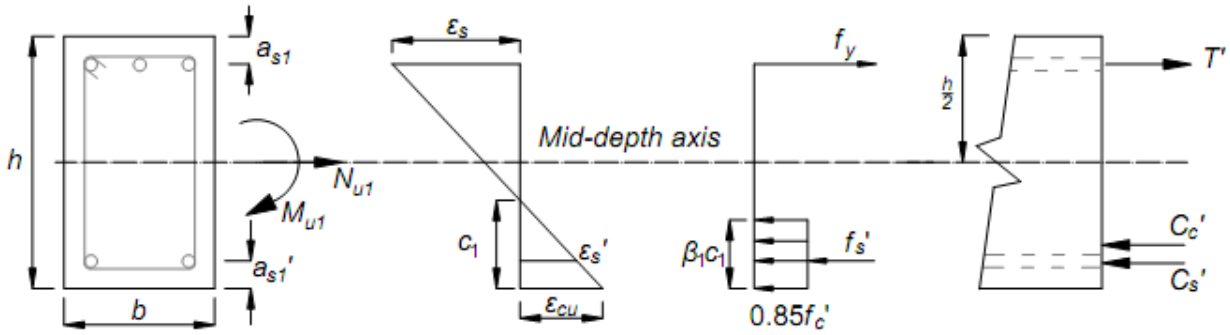

(a) Section and forces (b) Strain distribution (c) Stress distribution (d) Internal forces

Figure 5.7**:** Strain and stress distribution at a beam section (Yu and Tan, 2014)

Figure 5.7(d) shows that the beam axial force of a section is contributed by compression concrete, compression and tension reinforcement. Therefore,

$$N_{ul} = C_c' + C_s' - T \tag{5.14}$$

$$N_u = C_c + C_s - T \tag{5.15}$$

where $C_c^{'}$ and C_c are the concrete compressive forces, $C_S^{'}$ and C_s the steel compressive forces, and T' and T the steel tensile forces, acting on the beam ends and the middle joint interfaces, respectively. Based on Figure 5.7(c), $C_c^{'}$ and C_c can be calculated as

$$C_c^{'} = 0.85 f_c^{'} b \beta_1 c_1 \tag{5.16}$$

$$C_c = 0.85 f_c^{'} b \beta_1 c \tag{5.17}$$

where $f_c^{'}$ the compressive strength of concrete based on cylinder is tests, and β_1 is the ratio of the depth of the equivalent rectangular stress block to the neutral-axis depth.

According to Figure 5.7(b), the strains of compression and tension reinforcement at the beam ends are given by

$$\varepsilon_s^{'} = \left(1 - \frac{a_{s1}^{'}}{c_1}\right)\varepsilon_{cu} \tag{5.18a}$$

$$\varepsilon_s = \left(\frac{h - a_{s1}}{c_1} - 1\right)\varepsilon_{cu} \tag{5.18b}$$

where $a_{s1}^{'}$ and a_{s1} are the distances from the extreme compression fiber of concrete to the centroid of compression and tension reinforcement at the beam ends, respectively, and ε_{cu} is the ultimate compressive strain of concrete, assumed as 0.003.

After obtaining $\varepsilon_s^{'}$ via Eq. (5.18a), the compression reinforcement stress can be determined according to perfectly-elastic plastic constitutive model, the steel compressive force is given by

$$C_s^{'} = \varepsilon_s^{'} E_s A_s^{'} (if\ \varepsilon_s^{'} < \varepsilon_y) \tag{5.19a}$$

$$C_s^{'} = f_y A_s^{'} (if\ \varepsilon_s^{'} \geq \varepsilon_y) \tag{5.19b}$$

where ε_y the yield is strain of steel reinforcement and $A_s^{'}$ is the area of compression reinforcement. According to Figure 5.7(c), the force of tension reinforcement at the beam end is calculated as

$$T^{'} = f_y A_s \tag{5.20}$$

Since the tension reinforcement is at yield ε_s is greater than ε_y According to Eq. (5.18b), c_1 at the beam end should be less than

$$c_{yt1} = \left(\frac{h - a_{s1}}{1 + \varepsilon_y / \varepsilon_{cu}}\right) \tag{5.21}$$

Furthermore, the compressive and the tensile forces of reinforcement at the joint interfaces can be determined in a similar way as Eqs. (5.18) to (5.20), but they are expressed as functions of neutral axis depth c at the middle joint interface. Finally, according to Figure 5.7d), the bending moments M_{ul} and M_u at the beam ends and the joint interfaces can be determined with respect to mid-depth axis, respectively.

$$M_{ul} = C_c^{'}\left(\frac{h}{2} - \frac{\beta_1 c_1}{2}\right) + C_s^{'}\left(\frac{h}{2} - a_{s1}^{'}\right) + T^{'}\left(\frac{h}{2} - a_{s1}\right) \tag{5.22a}$$

$$M_u = C_c\left(\frac{h}{2} - \frac{\beta_1 c_1}{2}\right) + C_c\left(\frac{h}{2} - a_s^{'}\right) + T\left(\frac{h}{2} - a_s\right) \tag{5.22b}$$

where $a_s^{'}$ and $a_{s1}^{'}$ are the distances from the extreme compression fiber of concrete to the centroid of compression reinforcement, a_s and a_{s1} the distance from the utmost tension fiber of concrete to the centroid of tension reinforcement, at the beam ends and the joint interfaces, respectively.

Therefore, Force equilibrium condition gives one equation in terms of two unknowns c and c_1 independent δ, and compatibility condition produces the second equation (i.e., Eq. (5.12) in terms of c, c_1 and δ consequently, for a given δ, by solving these two non-linear equations simultaneously, the values of c and c_1 can be obtained. Subsequently, by substituting c and c_1 into Eqs. (5.13) to (5.12-5.22), one can obtain axial force N and bending moments M_u and M_{ul}. Substituting N, M_u and M_{ul} into Eq. (5.5) vertical resistance P can be determine.

Estimation of restraints stiffness

All restraints from the surrounding structure to a beam-column sub-assemblage can be converted to axial (K_a) and rotational restraints (K_r). Assuming the surrounding structure to be in elastic state, each restraint stiffness can be evaluated (see Appendix B). It is most likely that the restraint stiffness at the two ends of a sub-assemblage are not equal. For simplicity, the equivalent rotational stiffness is simply selected as the smaller stiffness of both ends because the weaker rotational restraint dominates the structural mechanism of a sub-assemblage.

5.3 Simplified Methods of Modeling Catenary Action (CA)

A catenary action analysis model was created to understand the mechanisms governing catenary action. A system of equations was developed by Orton (2007) to characterize the load and deflection relationship of a reinforced concrete beam in catenary action which was mention in literature review. In this study by modifying Orton (2007) model and including bar fracture and separating reinforcement bar strain of top and bottom reinforcement, catenary model is developed.

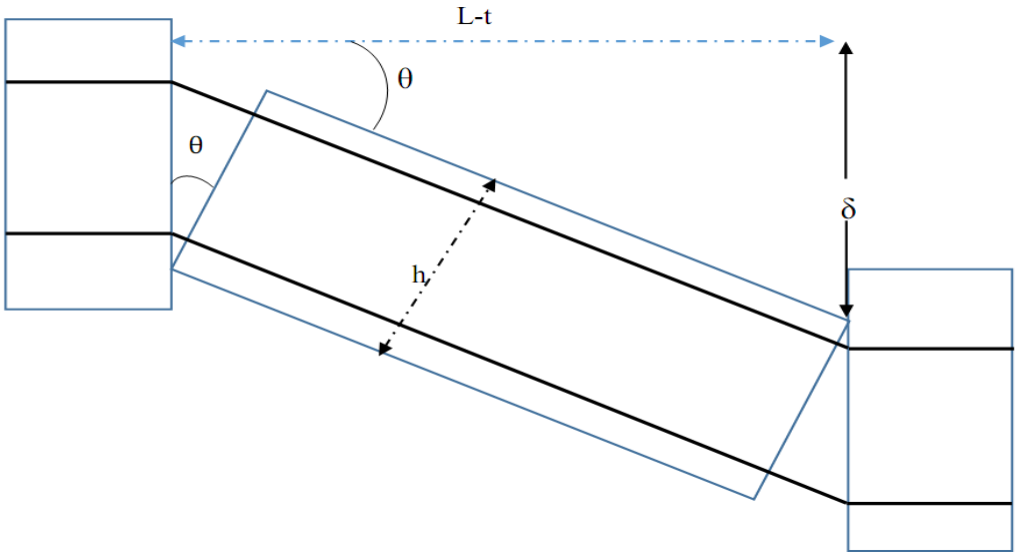

Figure 5.8: Beam deflation shape at catenary stage

Assumptions

- Perfect bond between concrete and steel bars
- beam modeled as a rigid rectangular blocks between the hinge locations and the length that experiences the elongation is the plastic hinge length only
- flexural capacity and effect of concrete is neglected in this stage.
- Strain value due to rotation consider until beam depth deflection after that only stain due to beam elongation is considered

Methodology steps

The model will be a displacement-controlled analysis. A vertical deflection is subjected to the system, and then the related axial force will be found by making use of the material

properties of steel. Finally, by using the compatibility and applying equilibrium equations, the vertical load related to the applied deflection can be found.

In order to determine the catenary response of the beam, the axial extension of the beam taken into account. The axial extension (δL) is due to rotation of the beam, support movement, and beam elongation. The components of axial extension can be determined from the applied loads and geometry of the beam. The elongated length of the beam is the hypotenuse of a right triangle with legs of the original length L and center displacement δ, Figure 5.9 .

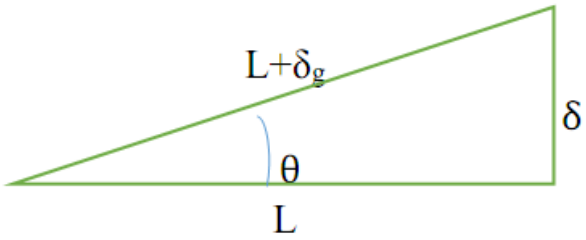

Figure 5.9: Deflection compatibility

$$(L+\delta g)^2 = L^2+\delta^2$$

$$L+\delta g = \frac{L^2+\delta^2}{L+\delta g} = \frac{L^2}{L+\delta g}+\frac{\delta^2}{L+\delta g} \quad \left(\text{Where } \frac{L}{L+\delta g}=\cos\theta, \frac{\delta}{L+\delta g}=\sin\theta\right)$$

$$L+\delta g = L\cos\theta+\delta\sin\theta$$

$$\delta g = \delta\sin\theta+L\cos\theta-L\ , \qquad \theta=\tan^{-1}\left(\frac{\delta}{L}\right) \tag{5.23}$$

- After the beam elongation is determined, calculate top and bottom strain of the reinforcements, due to elongation and rotation.

  Due to elongation $\varepsilon_E = \delta_g / L_p$ where ε_E is strain due to elongation and L_p is plastic hinge length. According to Paulay and Priestley the length of the plastic hinge can be obtained from the empirical formula as follows:

$l_p = 0.08l + 0.022 d_b f_y$, where l is distance from critical section to point of contra flexure, d_b is diameter of longitudinal reinforcement, and f_y is yield strength.

- Calculate top and bottom strain of the reinforcement due to rotation of the beam ε_R

  Strain due to rotation will be determined using triangular similarity from Figure 5.8

  then total strain will be $\varepsilon = \varepsilon_E + \varepsilon_R$.

- Determine the axial force capacity of the beam from idealized stress strain relation ship

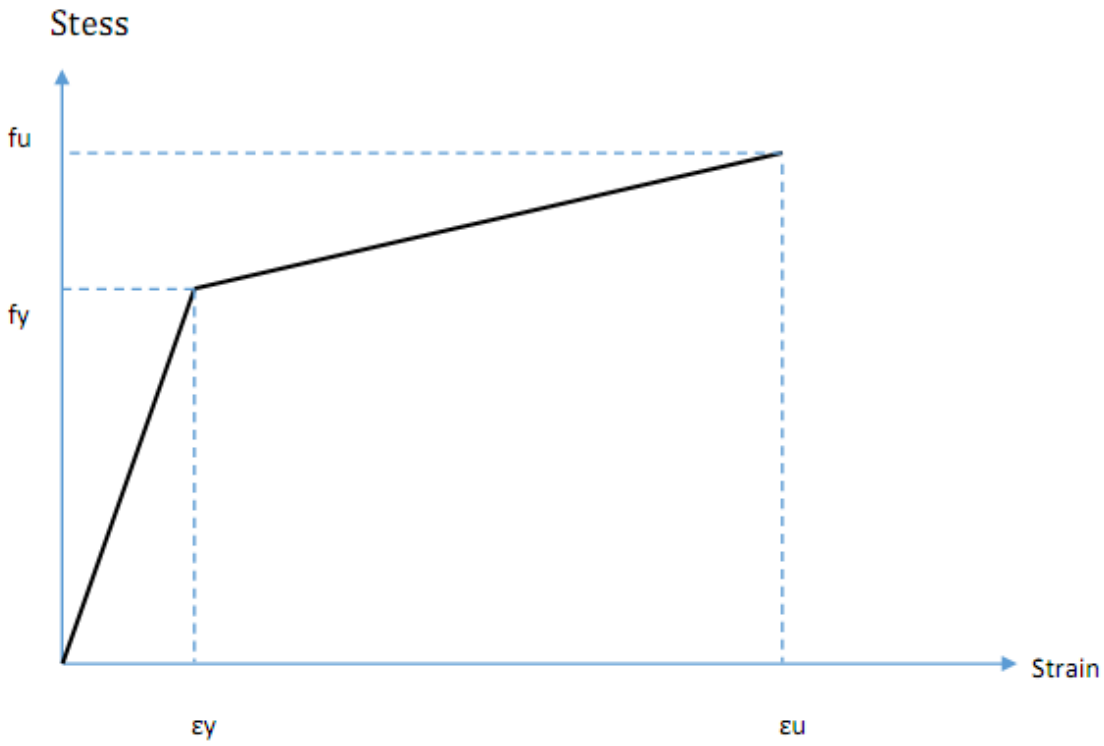

Figure 5.10: Idealized steel stress-strain model

$$f = \varepsilon * E_s \qquad \text{for} \quad 0 \le \varepsilon \le \varepsilon_y \qquad (5.24a)$$

$$f = \left(\frac{f_u - f_y}{\varepsilon_u - \varepsilon_y} \right) \left(\varepsilon - \varepsilon_y \right) + f_y \qquad \text{for } \varepsilon > \varepsilon_y \qquad (5.24b)$$

$$N_{top} = f \times A_{st}$$
$$N_{bottom} = f \times A_{sb} \quad (5.25)$$

where f stress at any strain ε, N_{top} and N_{bottom} top and bottom reinforcement axial force, A_{st} and A_{sb} are top and bottom reinforcement areas.

- Calculate vertical load caring capacity

$$P = 2N\sin\theta, \quad \text{where, } \sin\theta = \frac{\delta}{L+\delta_g} \text{ and } N = N_{top} + N_{bottom} \quad (5.26)$$

5.4 Bar Fracture

Bar fracture occur when steel strain equal or greater than ultimate steel strain. There are two possible scenarios for the sequence of bar fracture. The first scenario is that top steel bars at the beam ends and bottom steel bars at the middle joint fracture occurs at CAA stage. The second scenario is steel fracture occurs at CA stage. The location occurrence of fracture depends on depth of beam and ultimate steel strain capacity.

After top steel bars at the beam ends and bottom steel bars at the middle joint fractures, still the beam can carry additional vertical load by remaining bottom steel bar at beam end and top steel bar in middle joint as shown in Figure 5.12.

The axial load capacity after bar fracture will be:

$$N = f \times A_{s,ava} \quad (5.27$$

$A_{s,Ava} = \left(A_{st} + A_{sb}\right)/2$, where A_{st} and A_{sb} are top and bottom reinforcement area of middle joint and beam end respectively.

Vertical load caring capacity will be:

$$P = 2N\sin\theta, \text{ where, } \sin\theta = \delta/L+\delta_g \quad (5.28)$$

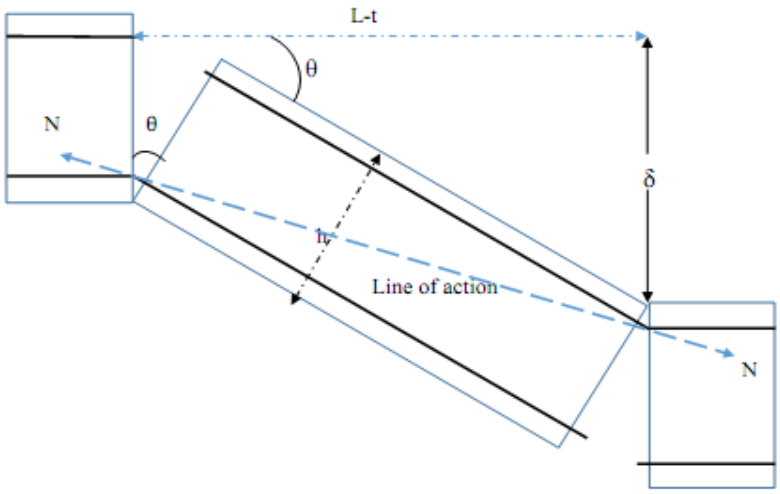

Figure 5.11: Deflected shape of single bay beam after bar fracture.

5.5 Result and Discussion

5.5.1 Evaluation of the proposed model

Before using the proposed model for studying effect of seismic provision levels in the development of CAA and CA capacity, it is required to verify the proposed model first. In order to verify the capability of the proposed models and equations to predict the structural behavior of RC beams at CAA and CA, a comparison with the available test result is performed.

The experiments used for evaluation were conducted on RC sub-assemblages consisting of two bay beams and three column stubs. Appendix C listed geometric, material properties and test results of all specimens used for comparison. Further information regarding the experimental test results can be found in the corresponding papers (Yu and Tan, 2013).

The Figure 5.12 and 5.13 show load-deflection (P-δ) relationship developed based on the analytical model of the sub-assemblages compare with experimental result. From experimental results of Orton (2007) and Yu and Tan (2013), when the middle joint of a sub-assemblage reaches around a displacement of one beam depth, it is likely that catenary action takes over CAA to sustain applied loads. Therefore, (P-δ) relationship for CAA stage are discussed with in the deflection range of 0.05d to one beam depth. And beyond beam depth CA stage discussed until complete bar fracture. The model can only be applied when sufficient vertical deflection has occurred to allow plastic hinges to develop at all critical sections.

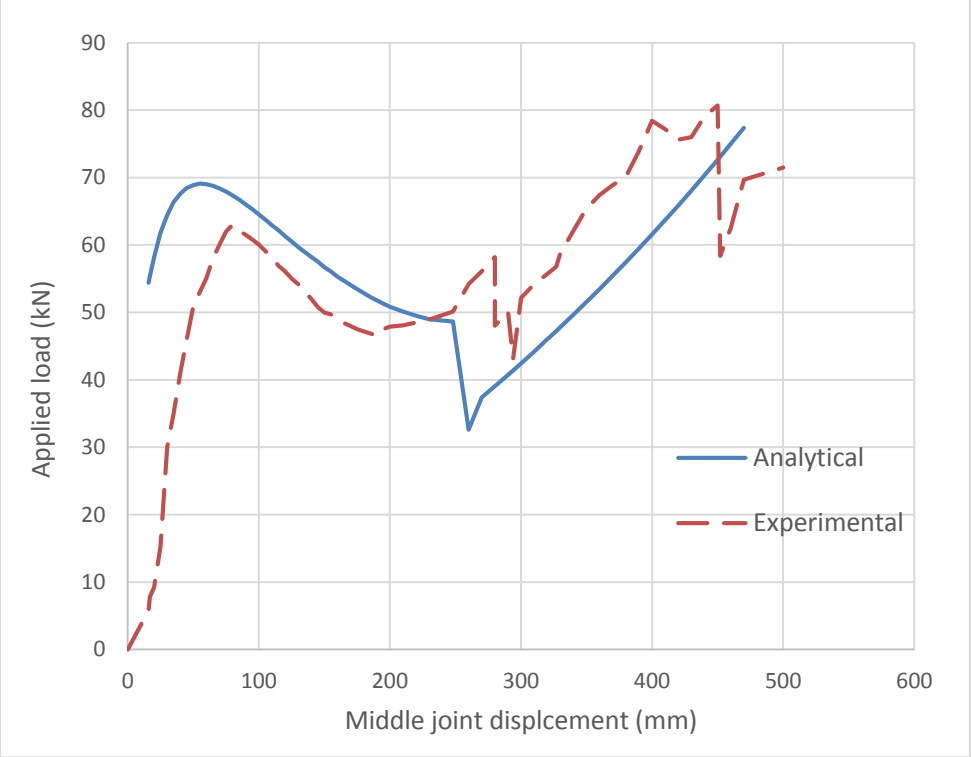

Figure 5.12: Comparison of analytical and experimental value for (Yu and Tan, 2013) S4

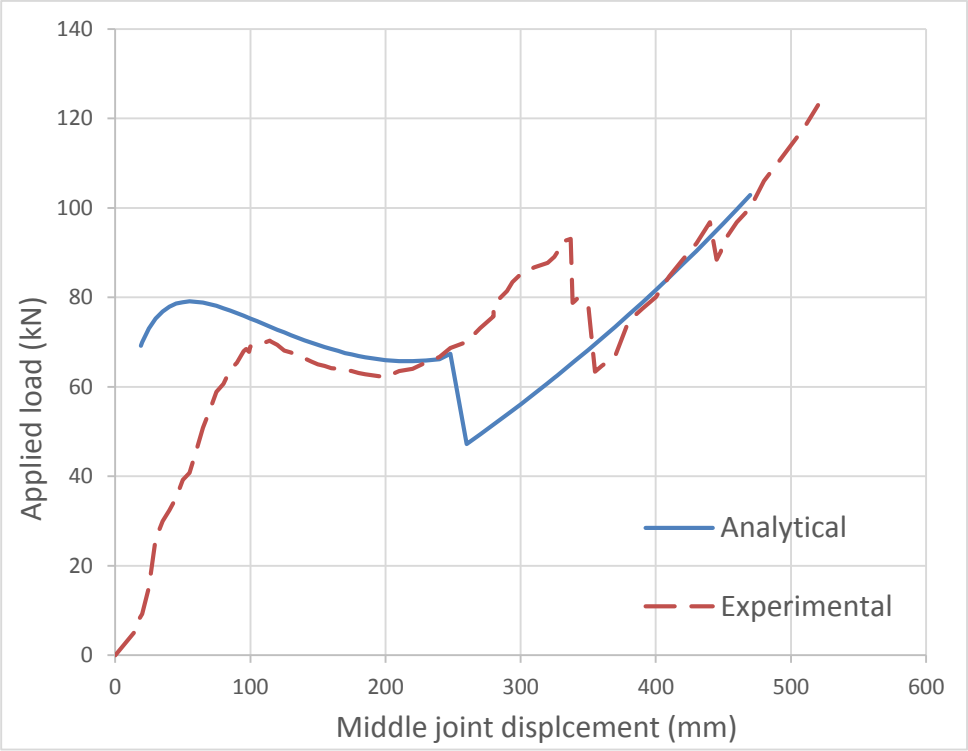

Figure 5.13: Comparison of analytical and experimental value for (Yu and Tan, 2013) S6

Table 5.1: Comparison of experimental and theoretical results for CAA and CA models.

Specimen (Yu and Tan, 2013)	Peak load at CAA(kN)	MJD at Peak load (mm)	Analytical (kN)	$\frac{Expermental}{Analytical}$	Load at CA max (kN)	MJD at P_{CA} (mm)	Analytical (kN)	$\frac{Expermental}{Analytical}$
S1	41.64	78	47.4	0.88	68.1	573	55.68	1.22
S2	38.38	73	44.2	0.86	67.63	612.0	48.8	1.32
S3	54.47	74.4	59.6	0.92	124.37	729.3	110	1.12
S4	63.22	81.0	65.5	0.97	103.68	614.3	82.47	1.21
S5	70.33	74.5	69.9	1.00	105.07	665.9	99.28	1.05
S6	70.33	114.4	73.47	0.96	143.28	675.3	134.2	1.06
S7	82.82	74.4	89.8	0.92	105.99	628.5	93.03	1.13

It can be seen from Figures 5.12 and 5.13 that the general trend of both analytical and experimental structural behavior was quite similar. CAA model slightly overestimates the capacity of RC beams, while the CA model slightly underestimates the capacity of RC beams at CA stage. This can be explained, during CAA stage the model assumes that the ultimate concrete strain remains constant as the deflection increases, which is in fact not the actual state as observed from experimental tests. The experimental tests showed that after the specimen attained its ultimate capacity concrete crushing has occurred, and caused to decreases CAA capacity. In other hand, In CA stage the occurrence of slip between the concrete and steel reinforcements, which is not considered in the proposed model, could allow steel stresses to penetrate through a larger length of steel reinforcement in tension, which cause an increase in CA capacity and delay bar fracture.

The first bar fracture occurred, in analytical study of (Yu and Tan, 2013) S4 and S6, at deflection of 248mm with fracture of bottom bar at middle joint and top bar at beam end. After that, the beam will took a form shown in Figure 5.11 until the remaining bars fracture followed, which occurred at 470mm. However, in the experiment result the first bar fracture occurred at bottom bar of middle joint with 283mm in S4 and 337.1mm for S6. And fracture of top bar at middle joint occurred at deflection of 614.3mm and 675.3mm for S4 and S6 respectively.

In general the difference between analytical and experimental curves could be related to the non-homogeneity of concrete, imperfection of beam construction, steel bar manufacture and unsymmetrical boundary conditions and loading. These parameters clearly affect the experimental results and failure modes such as sequence of bar fracture. Due to the effect of these parameters, the steel bars within the same layer fractured sequentially at different stages of deflection, which is clearly observed during the experimental testing. For ideal and perfect homogeneous conditions, the fracture of all steel bars within the same layer is expected to occur at one specific deflection, which is clearly reflected by the analytical curve.

5.5.2 Effect of seismic provision on the development of CAA and CA

To study effect of seismic design and ductility condition in the development of CAA and CA capacity, three continuous sub-assemblage beams are used to comparison, which are designed previously for low, medium, and high ductility classes. The beams occur above remove column location of the Cases (1, 2, and 4) mentioned Chapter 4. Since Case 3 is removal of corner column and CAA will not develop for cantilever beam, only removal of interior column effect is studied in here.

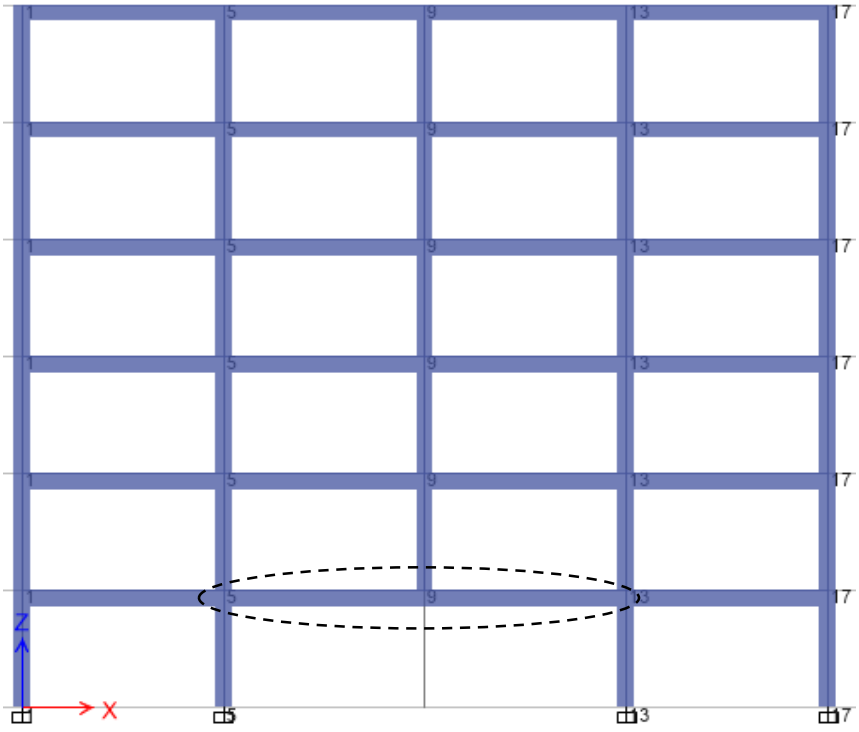

Figure 5.14: Location of analyzed beam

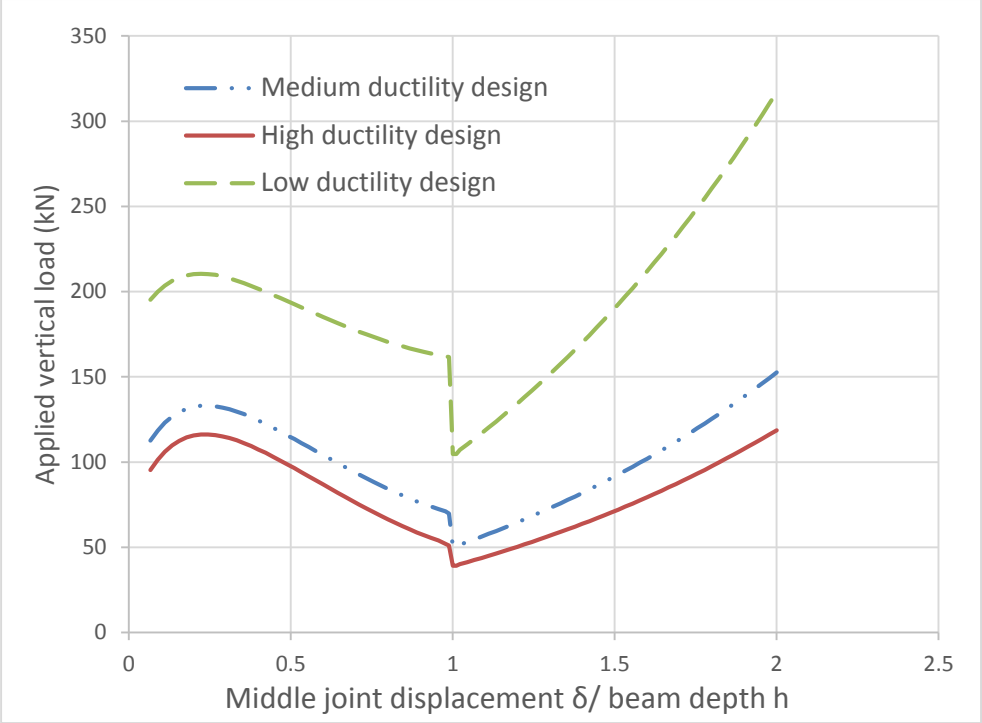

Figure 5.15: Load deflection relationship for Case 1

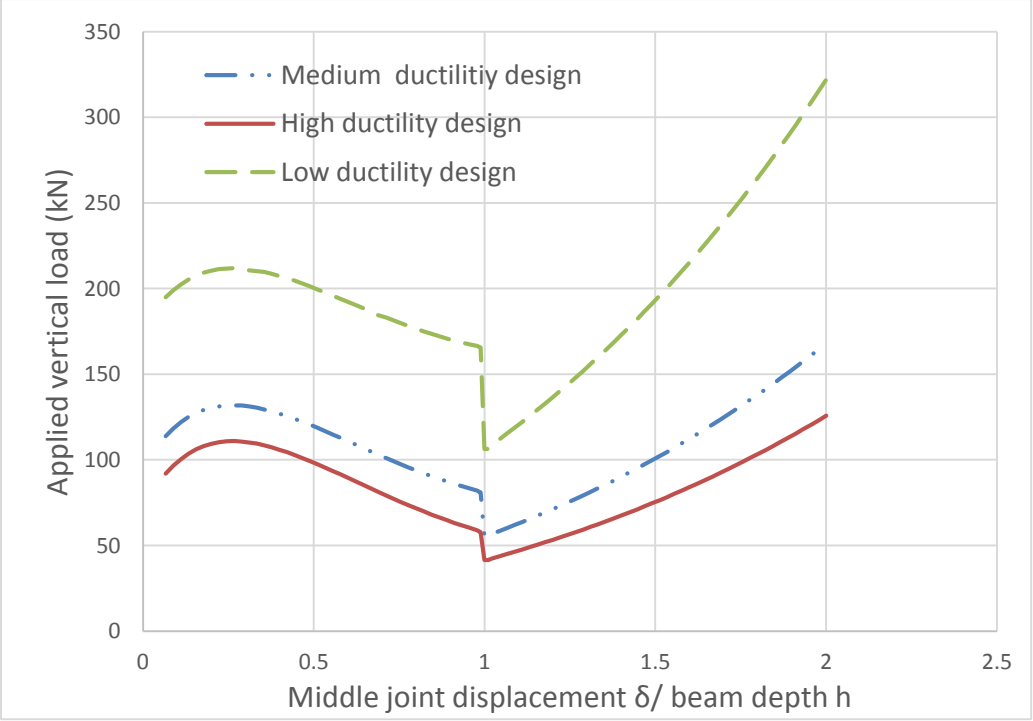

Figure 5.16: Load deflection relationship for Case 2

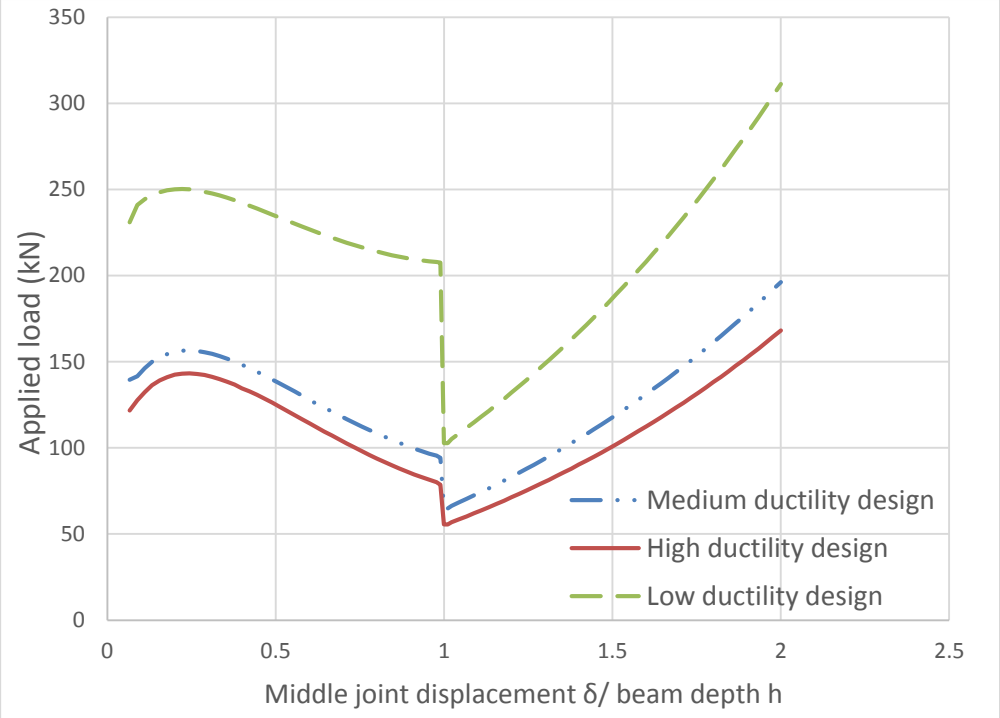

Figure 5.17: Load deflection relationship of Case 4

Table 5.2: Comparison of ductility class effect for CAA and CA capacity

Model	Maximum CAA (kN)			Maximum CA (kN)		
	Case 1	Case 2	Case 4	Case 1	Case 2	Case 4
High ductility design	116.27	110.97	143.21	116.22	123.05	164.56
Medium ductility design	133.02	131.87	156.62	149.32	164.45	192.09
Low ductility design	210.44	211.93	250.27	310.31	315.24	304.74

The Figures and Table above, shows that designing to low ductility class has higher CAA and CA capacity because low ductility class models had higher longitudinal reinforcement that provided from the seismic load, and which CAA and CA capacity highly depend on, therefore, decreasing ductility in the model increase CAA and CA capacity.

5.5.3 Application of compressive arch action (CAA) into design

Deformation corresponding to CAA capacity

Nonlinear modeling parameters and acceptance criteria for RC beams are explicitly provided in GSA guidance. If the rotation at a critical section corresponding to maximum CAA capacity of RC beams is within the acceptance criteria, then CAA can be used to effectively mitigate progressive collapse without excessive deformation.

Therefore, to check if CAA attain it maximum capacity with in the rotation limit provided by the guidance both experimental and analytical results are used. The experimental results of Yu and Tan 2013, and Alogla, K 2016 sub-assemblage tests result are used in this research. Total rotations θ_m corresponding to CAA capacity are computed by assuming all the plastic deformations are concentrated at two localized plastic hinges for each single-bay beam, Due to small deflection, total rotation θ_m at the critical sections is given by $\theta_m = \delta_a / l_n$ in which δ_a is the middle joint displacement of a sub-assemblage at CAA capacity and l_n is single span length of the beam. According to GSA 2013, for beams controlled by flexure, the nonlinear modeling parameters and acceptance criteria depend on reinforcement ratio indicator $(\rho - \rho')/\rho_{bal}$, provision of transverse reinforcement, and the ratio of applied shear force V to the shear strength provided by concrete only (i.e. $b_w d\sqrt{f_c'}$) at a section. The terms ρ and ρ' are tension and compression reinforcement ratios, respectively, and ρ_{bal} is the balanced steel ratio (MacGregor and Wight 2005). The terms b_w and d are the web width and the effective depth of beam section. In all the tests, the transverse reinforcement is categorized as nonconforming and $V/b_w d\sqrt{f_c'} \leq 3$. A component is conforming, if within the flexural plastic hinge region, hoops are spaced at $\leq d/3$. Otherwise, the component is considered nonconforming. For components of moderate and high ductility demand, the strength provided by the hoops is at least three-fourths of the design shear. (GSA 2013).

As shown in Table 5.3 and 5.4, all the specimens and analytical value, except one test result, can attain CAA capacity prior to reaching the specified deformation limit in acceptance criteria. Hence, based on the result CAA can be safely and confidently incorporated into design in accordance with the modeling parameters and acceptance criteria given by GSA 2013.

Table 5.3: Structural deformation corresponding to CAA capacity (experiment result)

Specimen	Length (mm)	CAA Peak load	Middle joint displacement at peak load	Rotation at peak load (θ_{caa})rad	Accepted Criteria Beam end (rad)	Accepted criteria Middle joint (rad)
S1	2750	41.64	78	0.028	0.045	0.06
S2	2750	38.38	73	0.026	0.047	0.06
S3	2750	54.47	74.4	0.027	0.042	0.06
S4	2750	63.22	81	0.029	0.045	0.06
S5	2750	70.33	74.5	0.027	0.05	0.06
S6	2750	70.33	114.4	0.041	0.038	0.06
S7	2150	82.82	74.4	0.035	0.045	0.06
S8	1550	121.34	45.9	0.03	0.045	0.06
SS1	2750	34.0	101.0	0.037	0.047	0.06
SS2	2750	37.9	96.8	0.034	0.047	0.06
SS3	2750	37.2	86.8	0.032	0.047	0.06
SS4	2750	36.7	91.4	0.033	0.047	0.06

Spacemen (S1-S8) are test result of Yu and Tan 2013 and (SS1-SS4) for Alogla, K 2017

Table 5.4: Structural deformation corresponding to CAA capacity (analytical result)

Model		Length (mm)	Middle joint displacement at peak load (mm)	CAA Peak load (kN)	Rotation at peak load (θ_{caa})rad	Accepted Criteria Beam end (rad)	Accepted criteria Middle joint (rad)
High ductility design	Case 1	5050	110	116.27	0.022	0.0610	0.063
	Case 2	5050	120.2	110.97	0.024	0.0611	0.063
	Case 4	5050	110	143.3	0.022	0.0618	0.063
Medium ductility design	Case 1	5050	109	133	0.022	0.0604	0.063
	Case 2	5050	120.2	132	0.024	0.0605	0.063
	Case 4	5050	109.93	156.55	0.022	0.0608	0.063
Low ductility design	Case 1	5050	100	210.44	0.02	0.044	0.05
	Case 2	5050	120	211.93	0.024	0.042	0.05
	Case 4	5050	100.2	250.27	0.02	0.042	0.05

Implementation of CAA into design

With plastic hinges occurring symmetrically at the middle joint interfaces and the beam ends, the corresponding flexural capacity p_f in the absence of beam axial force is given by $p_f = 2(M_f + M_{f1})/l_n$. Where M_f and M_{f1} are beam end and middle joint yield moments, l_n is a net span length of a single-bay beam.

With consideration of CAA, the structural capacity P_{caa} under a concentrated load is calculated as $p_{caa} = 2(M_u + M_{u1} - N\delta)/l_n$. Whereas M_u and M_{u1} are the ultimate moments of resistance at the middle joint interfaces and the end-column-stub interfaces due to the presence of axial force N and δ is the middle joint displacement.

The enhancement of structural resistance due to CAA, defined as $\mu = \left(P_{caa} - P_f\right)/P_f$

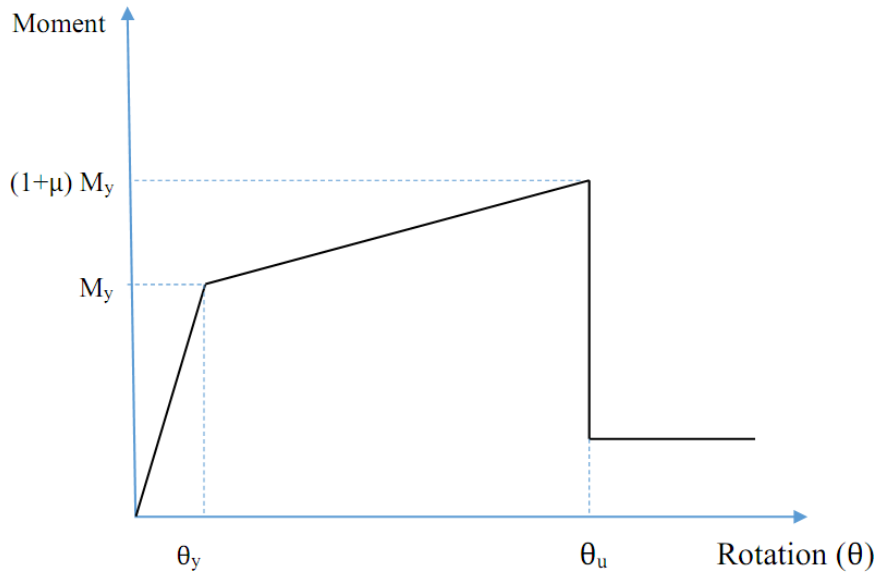

Figure 5.18 Moment-rotation relationship of a plastic hinge with CAA

If yielding moments at critical sections are multiplied by a coefficient of (1+μ) the corresponding ultimate flexural capacity is identical to CAA capacity. Accordingly, the moment-rotation relationship of a plastic hinge with consideration of CAA is shown in Figure 5.19.

To check effect of considering CAA capacity in analysis two external and internal planer frame building are considered, which was extracted from the building that is designed to medium and high ductility class. Nonlinear static (pushdown) analysis conducted considering CAA in the model with amplification factor in moment curvature relation as shown in the Figure 5.19, and compare with the frame that modeled without CAA capacity

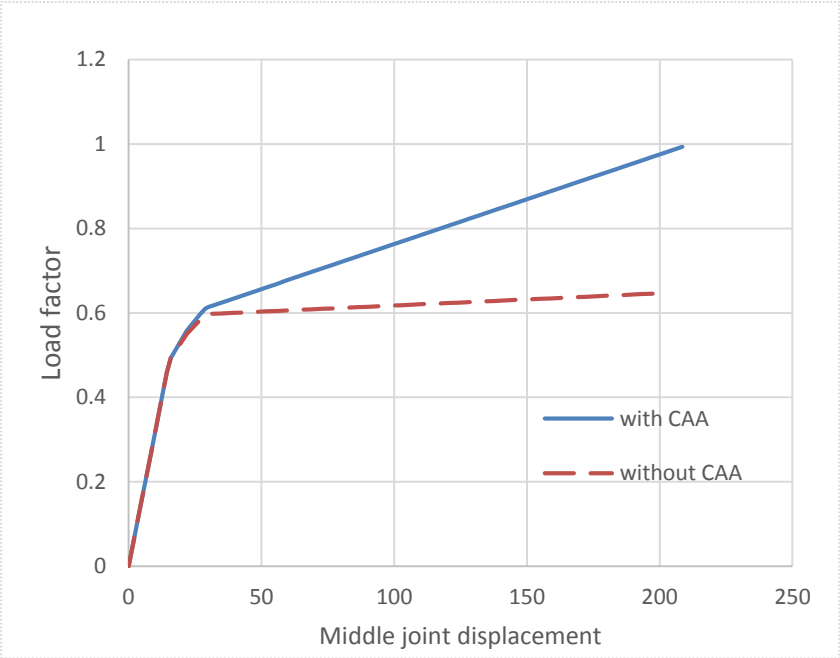

Figure 5.19: Pushdown of medium ductility design for Axis 1

Table 5.5**:** Considering with and without CAA

Model	Axis	Load factor (With CAA)	Load factor (Without CAA)	Percent of load increase
High ductility design	Axis 1	1.01	0.63	60.3%
	Axis 2	0.77	0.53	45.3%
Medium ductility design	Axis 1	0.99	0.65	52.3%
	Axis 2	0.74	0.51	45.1%

As comparison shown in Table 5.5 CAA has an average of 50% more flexural capacity. Moreover, CAA maximum capacity occurs prior to rotation limit provided by the GSA 2013 guidelines. Therefore, with adequate boundary restraints and shear strength, CAA can be incorporated into the alternative load path design method against progressive collapse.

CHAPTER 6 CONCLUSIONS AND RECCOMENDATIONS

6.1 Summary

To study the relationship between seismic provision and progressive collapse resistance both progressive collapse analysis of RC frame structure and analytical study on beam element were conducted. Before studying progressive collapse analysis, first a six-story regular RC framed models were designed with varying ductility classes according to ES EN 1998:1-2015. Ground accelerations of 0.15g with low, medium and high ductility classes were used. Moreover, a deficient structure with insufficient development length and lap splice at connection also was considered. Progressive collapse analysis was carried out on the four structures by considering four different column loss scenarios. Nonlinear static (pushdown) analysis were conducted in all 16 cases of progressive collapse assessment based on GSA 2013 guidelines.

For the GSA nonlinear analyses, flexural plastic hinges were assigned to the ends of the members. The hinge capacities were calculated based on section properties and the design ductility classes. Performance levels as defined by FEMA 356 (2000) were assigned to monitor the failure levels of the structures. The response of the structure including the maximum plastic rotations were monitored and compared with the acceptance criteria provided in the GSA 2013. It was observed that the loads from the removed columns were transferred to the adjacent columns through the connected beams by Vierendeel action resulting to significant increase in moments and moment reversals.

The displacement controlled pushdown analysis was carried out by increasing the applied load to increase the vertical displacement at the location of the removed column until collapse. By this, the ratios of the applied vertical loads at each step to the load of $\Omega_N \left[1.2D + 0.5L\right]$, which is known as load factor, were used for valuation.

During progressive collapse a beam adjacent to removed column undergoes different resistance mechanisms like Flexural, Compressive arch action (CAA) and Catenary action (CA). CAA and CA became the main resisting mechanisms against progressive collapse following a column loss. In this study the development of CAA and CA numerical model in RC beams became a main concern. The analytical study included assessing and modifying

the development of CAA and CA model and count in bar fracture as additional factor, then the model was evaluated and validated with the available experimental results. Moreover the analytical model used to study effect of seismic provision on progressive collapse resistance.

To investigate application of CAA into alternative path design first the rotation correspond to maximum CAA was compared with rotation limit provided by guideline, then effect of including CAA in the alternative path design was checked by using pushdown analysis through modifying moment-rotation relationship of the plastic hinge for frame with CAA.

6.2 Conclusion

The analyses carried out in this study came up with some major conclusions as elaborated below:

- Progressive collapse resistance of a structure is influenced heavily by the design ductility. From nonlinear pushdown analysis, Low ductility design had higher load factor when compared with Medium and High ductility design and this demonstrates that Low ductility design had better progressive collapse resistance.
- The plastic hinge rotations from nonlinear static analysis were found to vary according to the seismic design parameters. The average plastic hinge rotations calculated were 0.0466, 0.0405 and 0.0159 for High, Medium and Low ductility classes respectively.
- The location of removed column also influenced the progressive collapse susceptibility of the building. Removal of interior column (Case 4) was found to be most vulnerable. Whereas, removal of corner column (Case 3) was found to be most resilient to progressive collapse. Removal of interior column result in moment reversals in which beam design to negative moment exposed to positive action this makes interior column loss most vulnerable than corner column loss which has no moment reversal.
- When a critical column was removed, deficient structures with insufficient development length and lap splice at connection regions had difficulty in transferring applied loads to alternate load paths due to lack of strength and ductility. By comparing seismically designed (robust structure) and deficient structure, the importance of structural integrity was demonstrated. A seismically design building with good detailing exhibited more ductile behavior and larger load-carrying capacity than a deficient structure as predicted.

- In the analytical study, the comparison made between the experimental and analytical results shows that a reinforced concrete beams can be modeled as rigid rectangular blocks between the hinge locations to determine CAA and CA capacity.
- The analytical study shows that designing to Low ductility class has higher CAA and CA capacity, because Low ductility class Models had higher longitudinal reinforcement ratio that provided from the seismic load.
- From experimental and analytical result CAA was able to attain its maximum capacity before rotation limit reached, so CAA can be incorporated into the alternative load design method against progressive collapse via multiplying ultimate moments of resistance at critical sections by an enhancement factor.

6.3 Recommendation for Future Work

The research work presented in this thesis is based on investigation the response of a beam-column assembly of RC moment-resisting frame buildings due to the removal of a column. And this represents a further portion of possible cases for progressive collapse analysis of buildings. Given this, extra research is needed as summarized hereafter:

- Progressive collapse is a nonlinear and dynamic event. To more accurately evaluate the structural resistance against progressive collapse, it is necessary to conduct nonlinear dynamic analysis.
- In this thesis contribution of the concrete slab was not included. Therefore, it is required to study the effect of the slab stiffness on beam response for both progressive collapse analysis.
- Moreover, the analytical models can be improved by considering unsymmetrical boundary conditions and loading, strain rate, bar slip between concrete and reinforcement and reduction of beam effective depth for crushed concrete.

REFERENCES

Alogla, K. (2016). Progressive collapse resisting mechanisms of reinforced concrete . *Proceedings of the 5th International Conference on Integrity, Reliability and Failure*, p479-480.

ASCE 41-06. (2006). *Seismic Rehabilitation of Existing Buildings - American Society of Civil Engineers.* Reston: 1801 Alexander Bell Drive.

Babu, J. K. (2016). Progressive Collapse Resistance of Seismically Designed RC Framed Structures . *International Journal of Engineering Science and Computing*, 6 (7), p 8619-8624.

Corley, W. (1998). The Oklahoma city bombing: summary and recommendations for multihazard mitigation. *Journal of Performance of Constructed Facilities*, 12(.3), p100-112.

ES EN 1998-1. (2015). *Design of Structures for Earthquake Resistance.* Addis Ababa, Ethiopia: Ethiopian Building Code Standard prepared by Ministry of Works and Urban Development.

FEMA 356. (2000). *Prestandard and Commentary for the Seismic Rehabilitation of Buildings.* Washington,USA : Federal Emergency Management Agency.

FEMA, 227. (1996). *The Oklahoma City Bombing: Improving Building Performance.* Washington DC: Federal Emergency Management Agency.

GSA. (2003). *Progressive collapse analysis and design guidelines for new federal office.* Washington, D.C., USA: U.S. General Service Administration.

GSA. (2013). *Alternate path analysis and design guidelines for progressive collapse.* Washington, D.C. , USA: U.S. General Service Administration.

Hải, L. N. (2009). *Structural Response of Steel and Composite Building to Loss of Column, PhD.* de Liège: Université de Liège Faculté des Sciences Appliquées.

Ioani, A. G. (2013). Numerical Investigation of Progressive Collpase Resistance for Seismically Design Building. *Technical University of Cluj-Napoca Faculty of Civil Engineering*, P 124-126.

MacGregor, J. G., and Wight, J. K. . (2005). *Reinforced concrete Mechanics and Design.* Pearson Education, Inc.

NIST. (2007). *Best Practices for Reducing the Potential for Progressive Collapse in Buildings.* Washington, D.C: Department of Commerce.

Orton, S. (2007). *Development of a CFRP System to Provide Continuity in Existing Reinforced.* PhD Thesis, University of Texas at Austin, Austin.

Park, R. (1964). The ultimate strength and long-term behaviour of uniformly loaded, two-way concrete slabs with partial lateral restraint at all edges. *Magazine of concrete Research*, 16 (48): p139-152.

Pearson, C. (2005). Ronan Point Apartment Tower Collapse and its Effect on Building Codes. *J.Perform.Constr.Facil.*, 19(2), p172-177.

Priestley, T. P. (1992). *Seismic Design of Reinforced Concrete and Masonry Buildings.* New York: Jhon Wiley & Sons.

Rankin, G. I. (1997). Arching Action Strength Enhancement in Laterally Restrained Slab Strips. *Structures & Buildings 122*, Issue 4, pp. 461-467.

Sasani,M., and Kropelnicki, J. (2008). Progressive Collapse Analysis of an RC Structure. *The Structural Design of Tall and Special Buildings,*, 17, p757-771.

Yu, J., & Tan, K. H. (2014). Analytical model for the capacity of compressive arch action of reinforced concrete sub-assemblages. *Magazine of concrete research*, 66(3), 109-126.

Yu. J., and Tan,K. H. (2013). Structural behavior of RC beam-column subassemblages under a middle column removal scenario. *Journal of structural engineering, ASCE.*, 139(2), 233-250.

APPENDIX A: SIMPLIFICATION OF THE COMPATIBILITY EQUATIONS

A.1 For Equation 5.8

Substituting Equation 5.7 into Equation 5.6b, the following equation can be obtained.

$$\left[\beta l + 0.5\varepsilon(1-2\beta)l + (t+t_0)\right]\sec(\phi+\theta) = \left(\frac{h}{2}-c\right)\tan(\phi+\theta) + \left(\frac{h}{2}-c_1\right)\tan\phi + (1-\varepsilon)\beta l$$

Multiplying both sides by $\cos(\phi+\theta)$ and rearranging leads to

$$0.5\varepsilon l + (t+t_0) = \left(\frac{h}{2}-c\right)\sin(\phi+\theta) + \left(\frac{h}{2}-c_1\right)\tan\phi\cos(\phi+\theta) + (1-\varepsilon)\beta l\left[\cos(\phi+\theta)-1\right]$$

where, $\cos(\phi+\theta)-1 = -2\sin^2\left[(\phi+\theta)/2\right]$

further simplified as

$$0.5\varepsilon l + (t+t_0) = \left(\frac{h}{2}-c\right)\sin(\phi+\theta) + \left(\frac{h}{2}-c_1\right)\tan\phi\cos(\phi+\theta) - 2(1-\varepsilon)\beta l\sin^2\left(\frac{\phi+\theta}{2}\right)$$

Dividing both sides $\sin(\phi+\theta)$ then

$$c = \frac{h}{2} - \frac{0.5\varepsilon l + (t+t_0)}{\sin(\phi+\theta)} - (1-\varepsilon)\beta l\frac{2\sin^2\left[(\phi+\theta)/2\right]}{\sin(\phi+\theta)} + \left(\frac{h}{2}-c_1\right)\frac{\tan\phi}{\tan(\phi+\theta)}$$, which is the same us Eq. 5.8

A.2 For Equation 5.12

Since ϕ and θ are small, the trigonometric functions be replaced by equivalent infinitesimal mathematical terms. Also, the beam axial strain ε and the movements of the axial restraints $(t+t_0)$ are extremely small compared with l_n : Therefore

$$\sin\theta \approx \theta = M_{ul}/K_r$$

$$\tan(\phi+\theta) \approx (\phi+\theta)$$

$$\tan\phi = \phi$$

$$\sin(\phi+\theta) \approx 2\sin\left(\frac{\phi+\theta}{2}\right) \approx \phi+\theta = \frac{\delta}{l_n + 0.5\varepsilon b_j + (t+t_0)} \approx \frac{\delta}{l_n} = \frac{\delta}{\beta l}$$

$$\phi = \frac{\delta}{\beta l} - \frac{M_{ul}}{K_r}$$

Substituting the above equivalent values of the trigonometric

$$c = \frac{h}{2} - \frac{(0.5\varepsilon l + t)}{\delta}\beta l - \frac{\beta l t_0}{\delta} + \left(\frac{h}{2} - c_1\right)\left(1 - \frac{M_{ul}\beta l}{K_r \delta}\right) - (1-\varepsilon)\frac{\delta}{2}$$

Substituting $t = N/K_a$ and $\varepsilon = N/E_c\, A$ and rearranging

$$c = \frac{h}{2} - \frac{\delta}{2} - \frac{\beta l^2}{2\delta}\left(\frac{1}{bhE_c} + \frac{2}{lK_a}\right)N - \frac{\beta l t_0}{\delta} + \left(\frac{h}{2} - c_1\right)\left(1 - \frac{M_{ul}\beta l}{K_r \delta}\right)$$

APPENDIX B: ESTIMATION OF RESTRAINT STIFFNESS

The boundary restraint both rotation and axial stiffness of a two-bay beams are estimated based on Nam Hải (2009). According to Nam Hải the determination of partial rotational restraint and axial stiffness are discussed below.

B.1 Determination of partial rotational restraint coefficient K_S

To investigate the rotation stiffness of the beam end toward the adjacent members, the beam was physically replaced by a concentrated bending moment which appears at the beam end. Figure B.1 demonstrates the residual frame with a single bending moment applied to point C. The bending moment spreads out from point C and is distributed around the frame. As a result, the surrounding members are deformed.

Figure B.1 shows the members numbered in the order of the transferred rotations. From the beginning, point C is rotated due to the beam end's bending moment. Thus, the rotation reflects three adjacent members: C-1, C-2, and C-3. Likewise, the rotation of point 1 will produce the deformation of three adjacent components: 1'1, 1'2, and 1'3. The same types of behavior appear at points 2 and 3 to transfer to 2'1, 2'2, 2'3, then 3'1, 3'2, and 3'3, respectively.

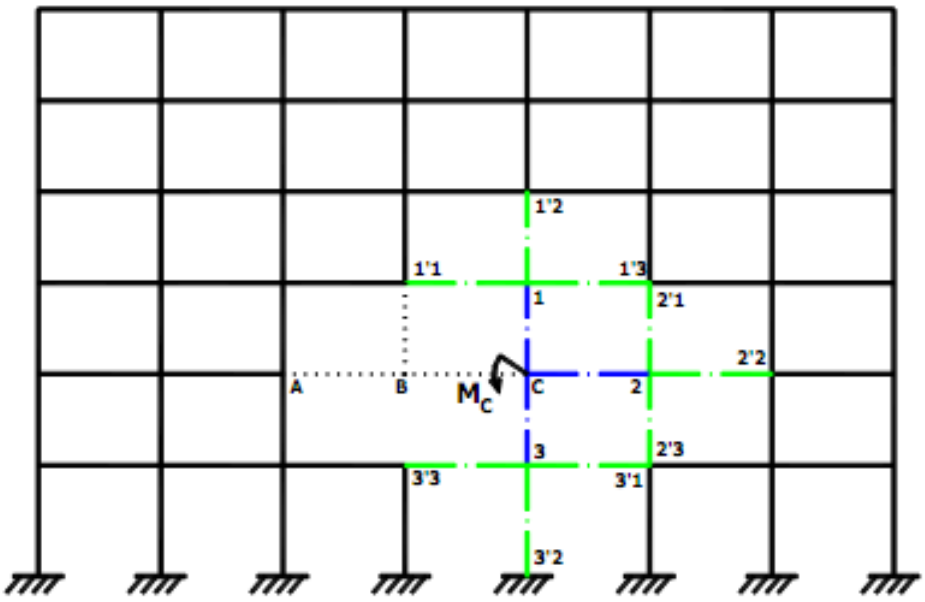

Figure B.1: Adjacent members in the spreading of bending moment (Hải, 2009)

After limiting the model to 2 transferred levels (in Figure B.1), the model was developed as in Figure B.2. The stiffness of a single beam undergoing a unit rotation at the beam end is S_B.The column's stiffness under the unit rotation at the column's end is likewise S_C.

$$S_B = \frac{4E_B I_B}{L_B} \qquad S_C = \frac{4E_C I_C}{L_C} \tag{B.1}$$

where E_B, E_C are the elastic moduli for beam and column, I_B, I_C are the inertia of the beam and column sections, and L_B, L_C are the beam and column lengths.

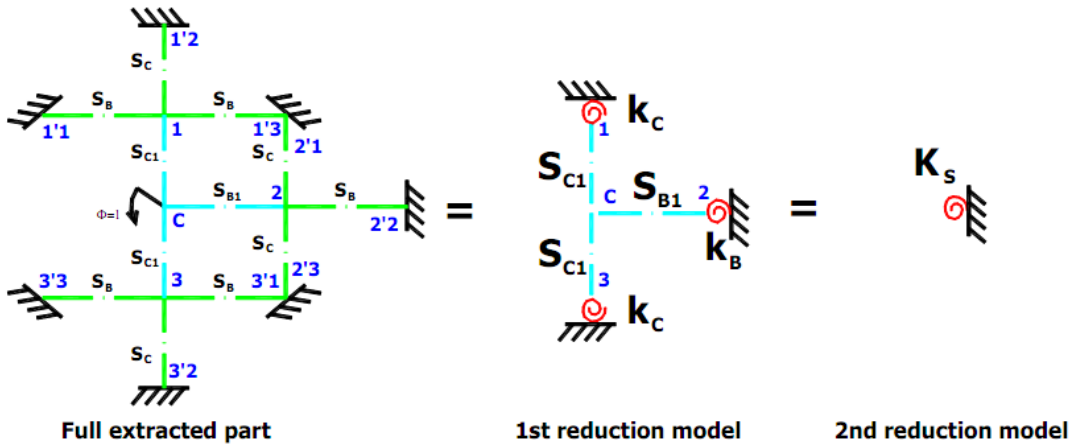

Figure B.2: Three levels development of at point C **(Hải, 2009)**

The rotational capacity K_C of point 1 is equal to the sum of three sources of bending stiffness: beams 1-1'1 and 1-1'3 and column 1-1'2. Called K_C because of its nature, this term represents the rotational stiffness of the end point for column C-1. This method is applied to point 2 to obtain the rotational stiffness K_B.

Continuing to the next level, the end condition of point 1 is applied to member C-1 by the end spring K_C. The bending stiffness of a member with an end spring condition is calculated below in Equation.

$$k_c = S_B + S_B + S_C \tag{B.2a}$$

$$k_B = S_C + S_B + S_C \tag{B.2b}$$

where k_C is the end rotational stiffness of columns C-1 and C-3, and

k_B is the end rotational stiffness of beam C-2.

The rotational capacity of partially restrained stiffness, point C, is the sum of the bending stiffness of 2 columns, C-1 and C-3, and the bending stiffness of the beam C-2. The columns' stiffness is S_{C1} and the beam's stiffness is S_{B1}.

$$S_{C1} = \frac{4E_C I_C}{L_C} \frac{L_C k_C + 3E_C I_C}{L_C k_C + 4E_C I_C} \quad \text{(B.3a)}$$

$$S_{B1} = \frac{4E_B I_B}{L_B} \frac{L_B k_{\mathbf{B}} + 3E_B I_B}{L_B k_B + 4E_B I_B} \quad \text{(B.3b)}$$

$$K_S = S_{B1} + S_{C1} + S_{C1} \quad \text{(B.4)}$$

where S_{C1}, S_{B1} are the bending stiffness of the column, beam with end's rotation spring, and

K_S is the partially restrained coefficient of point C.

B.2 Determination of axial stiffness

Figure B.3 illustrates the method for predicting the horizontal restraint coefficient. The movement of point 7 in Figure B.3, when supporting the axial force of the membrane beam, is limited by the stiffness of surrounding members as seen in the figure. That stiffness is mainly bordered by two floors: the one below and the one above the loaded floor.

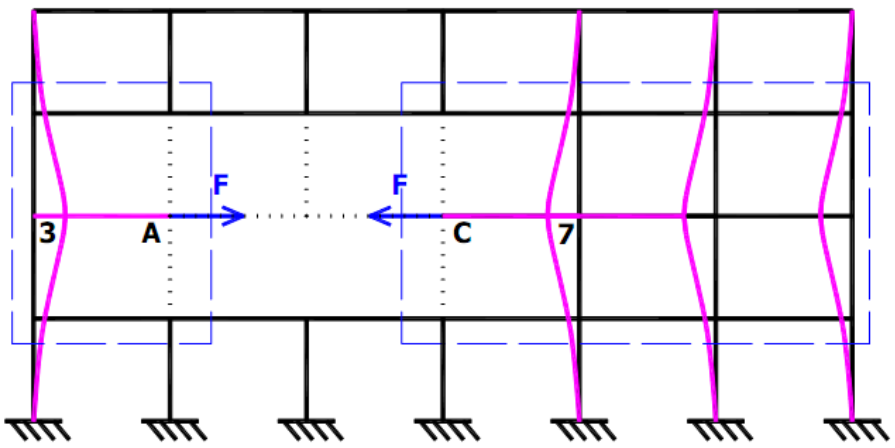

Figure B.3: Horizontal restraint definition **(Hải, 2009)**

The column supports a lateral force. As a result, it behaves like a beam instead of a column. So, as a beam, it undergoes a pure tensile and compressive force at the end. The beam section is elongated and shorten. In this way, it works as a member force.

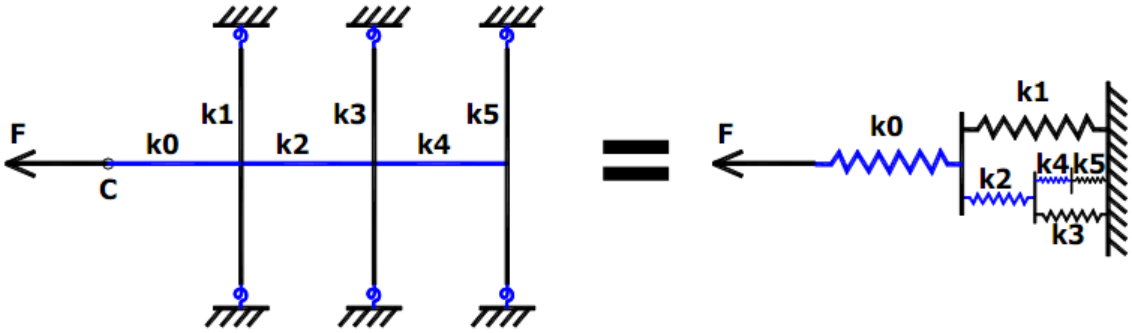

Figure B.4: The development of the model and its stiffness **(Hải, 2009)**

The model's stiffness was taken from the relation between the connected members. For example, the column's stiffness k_5 connects to the beam's stiffness k_4 at the loaded point, then the stiffness at equilibrium $k_{eq}(4,5)$ was obtained by the serial connection rule. Next, the column's stiffness was connected to the group (4,5) at the end of beam 4, then $k_{eq}(3,4,5)$ was treated as the group (4,5) parallel connected to column k_3. Consequently, the horizontal restraint coefficient K equals the total of group $(k_0, k_1, k_2, k_3, k_4, k_5)$.

$$\frac{1}{K} = \frac{1}{k_0} + \frac{1}{k_1 + \dfrac{1}{\dfrac{1}{k_2} + \dfrac{1}{k_3 + \dfrac{1}{\dfrac{1}{k_4} + \dfrac{1}{k_5}}}}} \tag{B.5}$$

where K the horizontal is restrained coefficient of point C, and k_i is the beam or column stiffness.

APPENDIX C: EXPERIMENT RESULTS USED FOR COMPARISON

Table C.1: Geometric properties of sub-assemblage specimens and experimental results of (Yu and Tan, 2013 & Yu and Tan, 2010)

Test No.	L_n (mm)	f_c (MPa)	Longitudinal reinforcement ratio (%)				Bottom bars at middle joints	Ultimate capacity (kN)	
			A-A section		B-B section			CAA	CA
			Top	Bottom	Top	Bottom			
S1	2750	31.2	0.90	0.49	0.49	0.49	continuous	41.64	68.1
S2	2750	31.2	0.73	0.49	0.49	0.49	continuous	38.38	67.63
S3	2750	38.2	1.24	0.49	0.82	0.90	lap-splice	54.47	124.37
S4	2750	38.2	1.24	0.82	0.82	0.82	continuous	63.22	103.68
S5	2750	38.2	1.24	1.24	0.82	1.24	continuous	70.33	105.07
S6	2750	38.2	1.87	0.82	1.25	0.82	lap-splice	70.33	139.9
S7	2150	38.2	1.24	0.82	0.82	0.82	continuous	82.82	105.99
S8	1550	38.2	1.24	0.82	0.82	0.82	continuous	121.34	59.58

- The beam sections are 150 mm wide and 250 mm deep for all specimens, i.e. b = 150 mm and h =250 mm; The concrete cover thickness was 20 mm for all specimens; total net span L=2Ln+250 (mm)

Table C.2: Geometric properties of sub-assemblage specimens and experimental results **(Alogla, 2016)**

Test No.	L_n (mm)	f_c (MPa)	Longitudinal Rein. Ratio (%)		CAA Ultimate Capacity (kN)	MJD (mm)	CA Ultimate Capacity (kN)	MJD (mm)
			Top	Bottom				
SS-1	2750	28.5	0.70	0.47	34.0	101.0	36.2	494.0
SS-2	2750	28.5	0.70	0.47	37.9	96.8	64.0	521.7
SS-3	2750	28.5	0.70	0.47	37.2	86.8	75.6	549.0
SS-4	2750	28.5	0.70	0.47	36.7	91.4	73.7	551.2

- The beam sections are 150 mm wide and 250 mm deep for all specimens.
- Further information regarding the experimental test results can be found in the corresponding papers.

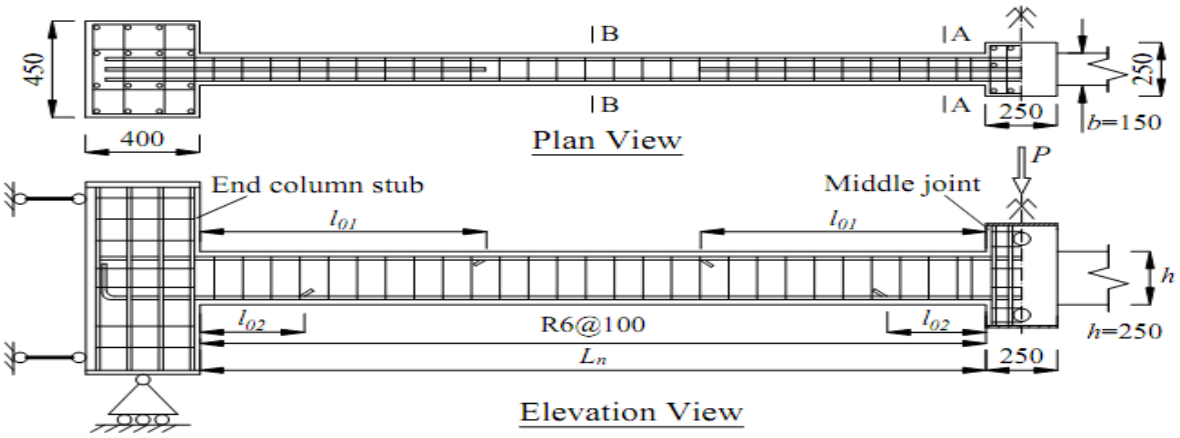

Figure C.1: Detailing and boundary conditions of specimens (Unit: mm) (Yu and Tan 2013)

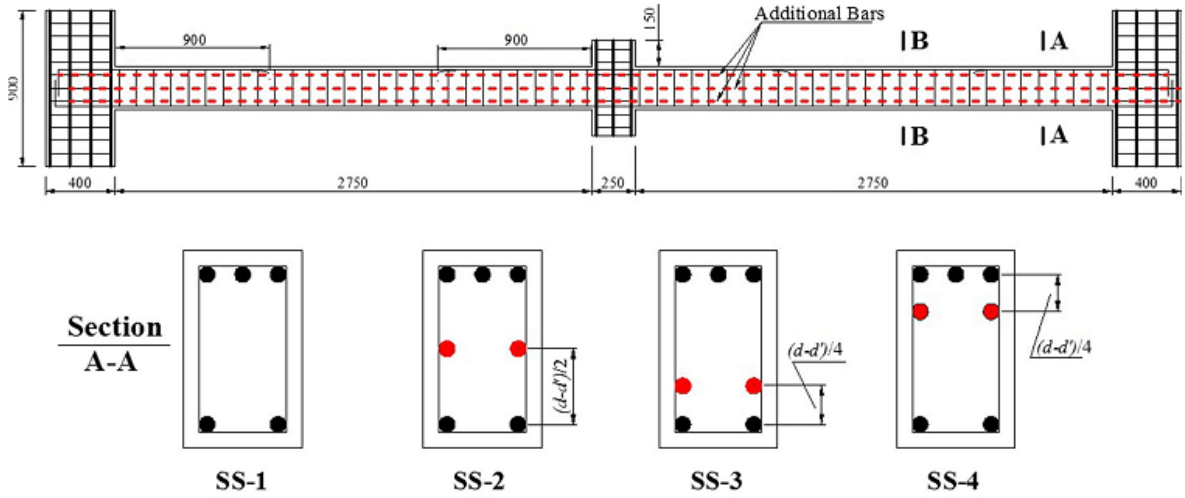

Figure C.2: Geometric properties of sub-assemblage specimens **(Alogla, 2016)**

APPENDIX D: AXIAL LOAD DISTRIBUTION BEFORE AND AFTER REMOVAL OF COLUMN

TableD.1**:** Axial load distribution before removal of column (kN)

Axis	A	B	C	D	E
1	660.2	1192.72	1196.65	1192.72	660.2
2	1172.83	2194.13	2182.24	2194.13	1172.83
3	1173.32	2174.1	2141.07	2174.1	1173.32
4	660.75	1174.06	1158.27	1174.06	660.75

Table D.2: Axial load redistribution for Case 1 (kN)

Axis	A	B	C	D	E
1	656.63	1646.92	**removed**	1646.92	656.63
2	1169.4	2204.92	2579.74	2204.92	1169.4
3	1175.07	2173.84	2115.17	2173.84	1175.07
4	637.67	1150.54	1135.67	1150.54	637.67

Table D.3: Axial load redistribution for Case 2 (kN)

Axis	A	B	C	D	E
1	1072.1	1195.22	1193.23	1197.55	639.19
2	**removed**	2586.48	2155.11	2196.66	1147.95
3	1616.05	2184.53	2139.05	2175.78	1153.88
4	659.89	1177.24	1160.02	1172.18	638.49

Table D.4**:** Axial load redistribution for Case 3 (kN)

Axis	A	B	C	D	E
1	**removed**	1575.82	1193.56	1212.36	659.62
2	1549.28	2200.32	2179.07	2194.22	1153.54
3	1172.6	2172.67	2142.72	2176.83	1152.82
4	659.05	1148.49	1137.34	1157.87	622.41

TableD.5**:** Axial load redistribution for Case 4 (kN)

Axis	A	B	C	D	E
1	655.61	1206.8	1715.97	1206.78	655.63
2	1136.88	2758.47	**removed**	2758.45	1136.89
3	1170.65	2192.96	2703.61	2192.96	1170.65
4	663.14	1173.75	1124.5	1173.45	663.14

APPENDIX E: VERIFICATION OF PUSHDOWN ANALYSIS USING ETABS

To verify pushdown analysis a six story plane frame building was used, which is previously designed to medium ductility class in Chapter 3. Incremental (hand calculation) progressive analysis conducted by increasing the gravity load until plastic hinges formed. Then compare with the ETABS output as shown in the Figure A.7.

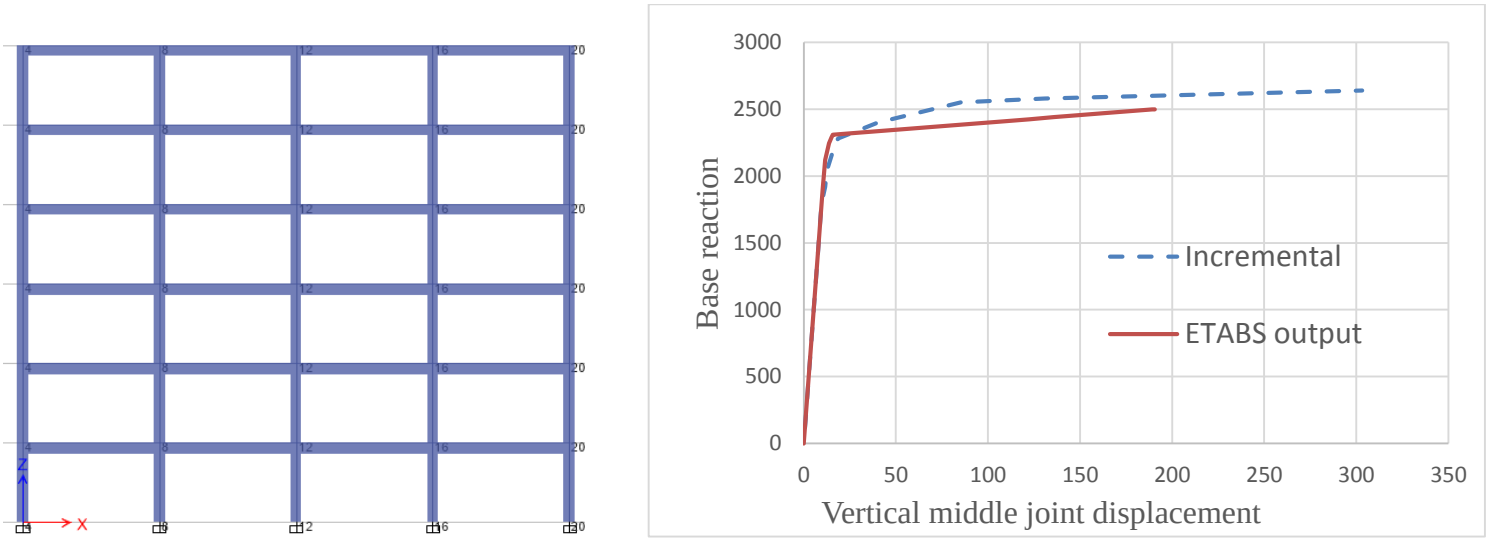

Figure E.1: (a) Plan frame used for verification (b) Base shear vs middle joint displacement

From the verification analysis shown in the figure A.7, in both cases the sequence of hinge formation is quite similar, however, the incremental (hand calculation) had higher base reaction and displacement value when compare with ETABS output. This is because ETABS is built in pushdown analysis with options including hardening/loss of strength, P-M interaction and Systematic stiffness approach which is not included in this incremental analysis.